

PNNL-38433

Assessment of Benefits of Solid-State Advanced Manufacturing Processes for Nuclear Energy Products

M3CR-22PN0402024

September 2025

Isabella van Rooyen Carolyne Burns Mageshwari Komarasamy Asif Mahmud Ramprashad Prabhakaran Kenneth Ross Tianhao Wang Mayor Pole David Garcia



DISCLAIMER

This report was prepared as an account of work sponsored by an agency of the United States Government. Neither the United States Government nor any agency thereof, nor Battelle Memorial Institute, nor any of their employees, makes any warranty, express or implied, or assumes any legal liability or responsibility for the accuracy, completeness, or usefulness of any information, apparatus, product, or process disclosed, or represents that its use would not infringe privately owned rights. Reference herein to any specific commercial product, process, or service by trade name, trademark, manufacturer, or otherwise does not necessarily constitute or imply its endorsement, recommendation, or favoring by the United States Government or any agency thereof, or Battelle Memorial Institute. The views and opinions of authors expressed herein do not necessarily state or reflect those of the United States Government or any agency thereof.

PACIFIC NORTHWEST NATIONAL LABORATORY

operated by

BATTELLE

for the

UNITED STATES DEPARTMENT OF ENERGY

under Contract DE-AC05-76RL01830

Printed in the United States of America

Available to DOE and DOE contractors from the Office of Scientific and Technical Information, P.O. Box 62, Oak Ridge, TN 37831-0062

www.osti.gov ph: (865) 576-8401 fox: (865) 576-5728 email: reports@osti.gov

Available to the public from the National Technical Information Service 5301 Shawnee Rd., Alexandria, VA 22312 ph: (800) 553-NTIS (6847) or (703) 605-6000

email: info@ntis.gov
Online ordering: http://www.ntis.gov

Assessment of Benefits of Solid-State Advanced Manufacturing Processes for Nuclear Energy Products

M3CR-22PN0402024

September 2025

Isabella van Rooyen Carolyne Burns Mageshwari Komarasamy Asif Mahmud Ramprashad Prabhakaran

Prepared for the U.S. Department of Energy under Contract DE-AC05-76RL01830 Kenneth Ross Tianhao Wang Mayor Pole David Garcia

Pacific Northwest National Laboratory Richland, Washington 99354

Summary

The Advanced Materials and Manufacturing Technology (AMMT) program develops cross-cutting technologies in support of a broad range of nuclear reactor technologies and maintains U.S. leadership in materials and manufacturing technologies for nuclear energy applications.

This research is focused on development of advanced processing routes for high-performance nuclear materials (e.g., oxide dispersion strengthened [ODS] alloys) that offer high-temperature and radiation-resistant capabilities, while remaining cost-effective and scalable for bulk and/or mass production. Expected outcomes include demonstration of viable manufacturing pathways, a science-based understanding of material behavior, and early-stage validation of candidate materials for future reactor deployment. New materials with improved mechanical properties and service life through solid phase alloying and grain refinement, will make an impact on the new advanced reactor deployment and therefore address the overarching vision of AMMT program.

Solid-state advanced manufacturing techniques can overcome some of the challenges in liquid-based additive manufacturing (AM) processes and therefore should be considered in material design and manufacturing as well. The work presented in this report forms part of a study on solid-state AM techniques of 316 stainless steels (SS) and ODS steel components and supports the vision and goals of the AMMT program relevant to accelerate the development and deployment of advanced manufacturing processes. Achieving this can provide safety improvement through larger safety margins, economic benefit for higher efficiency during operation, and a cost reduction through more effective manufacturing processes and less waste.

This overall project provides the U.S. Department of Energy a critical feasibility study comparison of three solid-state processes to other AM processes, thereby providing the feasibility of the solid-state processes examined to manufacture 316H SS and ODS steel components:

- Fused-filament fabrication (FFF): This work provides an initial evaluation of the impact of powder morphology and sizes on the FFF process, and the feasibility and adaptability for different material systems, to use FFF for ODS steels and 316 SS.
- Shear-assisted processing and extrusion (ShAPE): Specifically for this portion of the project
 on ShAPE tube forming, the objectives will be to determine the feasibility to direct tube
 forming of high tensile strength steel tubing, specifically for ODS steel to determine the
 effect of the patented extrusion process on the dispersoids of the ODS material.
 Additionally, as often ODS powders are mechanically alloyed and therefore more platelike or
 angular, this feasibility was to explore the impact on the optimization process and initial
 feasibility of direct tube forming.
- Cold spray and friction stir additive manufacturing as a stretch goal: Bulk and near net shape manufacturing processes for high-temperature, high-strength alloys are needed. Additionally, cold spray techniques can be applied in-situ at the operational level for repair and can provide multiple benefits to the nuclear industry. These tasks aim to provide information to show benefits of cold spray during the full life cycle, namely research and development, product manufacturing, and repair to mention a few key points.

ContentsSummary

Development of the FFF process and the research results provide evidence that it is feasible to print ODS steel as well as 316H SS using the solid-state FFF process. Both ODS steel and 316H SS custom filaments were successfully fabricated with a powder loading of 65% and 62%, respectively. Specific filament fabrication and printing parameters for each material type and powder were determined to achieve successful printing and therefore show feasibility to use FFF for component manufacturing and capability at Pacific Northwest National Laboratory. However, process optimization for fully dense parts is necessary and the scalability needs further work. The filament fabrication process and printing are sensitive for the powder morphology, size, and size distribution mainly due to the flowability of filament extrusion as well as sinter effectiveness. A significant benefit is that custom powder can be used for FFF, so an in-house capability was developed enabling ODS and 316H SS powder loading techniques. This may lead to an advantage when designing new material compositions for specific applications. Although effective printing and subsequent sintering did occur, further optimization is needed to fully fabricate structural sound components.

This study provides first-of-a-kind results of direct tube formation using the ShAPE process for ODS steel material; previously only the bar form was successfully made. Previously only bar shapes have been successfully made. This study provides preliminary information on development of ShAPE tube forming of ODS directly from stock material, and not via an interim step of bar and pilgering as one of the current manufacturing methodologies. The first ShAPE experiment completed on the PM2000 billet yielded an approximately 4-inch length of tube and shows in principle the feasibility of the direct tube fabrication in a single step while recognized that full steady-state conditions were not reached during the first experiment, and that process optimization should still be performed on this specific material conditions. A detailed microstructural analysis, although showing variations between the start, middle and end sections, shows that conditions towards the end were more consistent and can be built upon during next studies. However, the results, both in understanding the process parameters and behavior in relationship with the microstructural variations, can provide valid input to the modeling efforts, although not funded under the AMMT program, can minimize future experiments. The number density of precipitates shows an inverse proportionality to the change of their size, except for the bulky square-type aluminum-rich precipitates mostly identified at the end section of the ShAPE sample. The increase in the precipitate size and decrease in density suggest ShAPE-induced growth of the secondary oxide particles without significantly affecting the overall level of oxidation. This suggests that ShAPE might be used to refine ODS particles, but further experimentation is required to verify this observation. However, the moderate size and the highest density of bulky square-type precipitates observed at the end section of the extruded sample also suggest ShAPE-induced increase in the second phase precipitation.

Compared to the wrought PM2000, all the experiments with spark plasma sintered (SPS) Billets as feedstock for the SHAPE tube fabrication process had resulted in fractured tubes. This could be due to the porosity in the SPS consolidated feedstocks. An early conclusion is therefore that the stock material for the current feasibility shows that less than 97% dense feedstock is not sufficient for ODS materials for direct tube forming. However, another aspect that needs to be considered that has not been established, is how the bimodal grain sizes influence the consistency and flow during the extrusion process. Characterization of these extrudates could not yet be performed to determine if there are any differences in the ODS particle size or distributions after being exposed to the combined effect of SPS and ShAPE extrusion. Specifically, the third experiment using SPS billet 4 did not reach steady state; therefore, the microstructure resulting would not provide conclusive evidence yet.

ContentsSummary

Finally, the four ShAPE experiments conducted show feasibility regarding fabricability for ODS tube forming was shown, although optimization for microstructure repeatability would need to receive attention with follow-up work; therefore, the combination of results reported here, together with the separate studies by other PNNL researchers on bar fabrication of ODS, provide the justification for 3 to 4 Technical Readiness Level feasibility.

Although the cold spray and friction stir surfacing experiments were performed as a smart goal with limited resources, the benefits of these processes were noted in the results. The initial CS experiments using 316H powder size (like laser powder directed energy deposition powder) were not sufficient to provide a full bonded structure. However, alternating CS with friction stir processing resulted in an inherent bonded and dense structure. The application of additive friction surfacing was demonstrated and shows promise for future near net shape manufacturing and bulk manufacturing of high strength and high temperature materials. Specifically, the equiaxed ultrafine grain structure produces improved properties and corrosion resistance based on previous results. The first attempt reduced grain size from ~27 to ~2 - 4 µm and it is expected that ~1 to 1.5 µm is achievable with process optimization. Results show that additive friction surfacing is a feasible method for near net shape large-scale additive manufacturing of nuclear components with improved properties and cost compared to competing techniques. Specifically, it was noted that conditions exist where the interlayer boundaries are not readily visible, therefore predicted homogenous properties for bulk manufacturing applications. The optimization processes will need to address tool-material interactions and the structural integrity of the tooling to prevent any secondary inclusions.

Finally, a matrix for potential applications based on performance and/or requirements is provided in this report. Feasibility of applying solid state techniques for high temperature and high strength materials applicable to the nuclear industry was demonstrated using three methods and two material types that is currently sought after by the nuclear industry. It is recommended that this work is continued in selected component and applications domain, so that process optimization can be developed and therefore have an impact based on increased level of technology readiness. It is further recommended that the different solid state manufacturing process needs to be considered during the early design stages as well, as these processes provide a significant economic and sustainable benefit.

ContentsSummary

Acknowledgments

The research presented here was supported by the Advanced Materials and Manufacturing Technologies Program of the Department of Energy's (DOE's) Office of Nuclear Energy. Pacific Northwest National Laboratory (PNNL) is a multiprogram national laboratory operated for DOE by Battelle Memorial Institute under Contract No. DE-AC05-76RL01830. The authors thank Subhashish Meher for the peer review of the report and Cary Counts for the technical editing of the report.

Acknowledgements for material and services collaboration and support:

- PNNL would like to thank Dr Xuan Zhang (Argonne National Laboratory) for providing us with the 316H stainless steel powder (Batch 2) used in the FFF study.
- Dr T.S. Byun from Oak Ridge National Laboratory is thanked for providing the smaller than 325 mesh 14YWT (Batch 2) material.
- PNNL would like to thank Dr Sebastien Dryepondt from Oak Ridge National Laboratory for providing us with the PM2000 forged billet used in this study.
- We would like to acknowledge Dr. Stuart Maloy, Dr. David Hoelzer, and Prof. G. Robert
 Odette for providing the 14YWT powder (called Batch 1) with this study. The production of
 the 14YWT powder was funded by the DOE Global Nuclear Energy Partnership program in
 2008 subcontract-70553-001-09.
- Drs, Michael McMurtrey, Xinchang Zhang and Jorgen Rufner are thanked for the execution of spark plasma sintering densification of the 14YWT Batch 1 powder.

Specific acknowledgment for the authors of the prior milestone reports summarized in this report:

- Carolyne A Burns, Saumyadeep Jana, Amrita Lall, Zachary C Kennedy, Michelle D Fenn, Joshua A Silverstein, Lorraine M Seymour, Isabella J van Rooyen; "Preliminary Characterization and evaluation on FFF Manufactured 316H and ODS Steels", PNNL-34985, September 2023, (Burns et al. 2023).
- Isabella van Rooyen, Mageshwari Komarasamy, Chinthaka Silva, Shalini Tripathi, Julian Atehortua, Mayor Pole, Tanvi Ajantiwalay, David Garcia, Quin R S Miller, Matthew Olszta, Ramprashad Prabhakaran, Tianhao Wang; "Preliminary Characterization and Evaluation on ShAPE Manufactured 316H and ODS Steels", M3CR-22PN0402023, PNNL-36737, September 2024, (Van Rooyen et al. 2024)

Acronyms and Abbreviations

AFS additive friction surfacing
AM additive manufacturing

AMMT Advanced Materials and Manufacturing Technology

CS cold spray

EBSD electron backscatter diffraction

EDS electron dispersive X-ray spectroscopy

FFF fused-filament fabrication

FSAM friction stir additive manufacturing

FSP friction stir processing
FSW friction stir welding
HAZ heat affected zone

HPCS high pressure cold spray LPCS low-pressure cold spray

LSAM large-scale additive manufacturing

NNS near net shape

Ni nickel

ODS oxide dispersion strengthened
ORNL Oak Ridge National Laboratory

OM optical microscopy

PCBN polycrystalline cubic boron nitride

PNNL Pacific Northwest National Laboratory

R&D research and development

RPM revolutions per minute

SEM scanning electron microscopy

ShAPE shear-assisted processing and extrusion

SPS spark plasma sintered

SS stainless steel

TEM transmission electron microscopy

Contents

Sumr	nary			ii
Ackno	owledgr	nents		v
Acror	nyms an	ıd Abbrev	/iations	v i
1.0	Introd	luction		13
	1.1	Project	Objectives and Overview	13
	1.2	Work S	Scope	14
2.0	Toward Additive Friction Surfacing of Stainless Steel 316-H for Large-Scale Additive Manufacturing			15
	2.1	Iterativ	e High Pressure Cold Spray and Friction Stir Processing	15
		2.1.1	Cold Spray Process Description	15
		2.1.2	Friction Stir Processing Process Description	16
		2.1.3	Experimental Method	17
		2.1.4	Results	18
	2.2	Additiv	e Friction Surfacing	22
		2.2.1	Additive Friction Surfacing Process Description	22
		2.2.2	Experimental Procedures	23
	2.3		sions and recommendations on Cold Spray and Additive Frictioning	26
3.0	Preliminary Characterization and Evaluation on FFF Manufactured 316H and ODS Steels: Summary			27
	3.1	Background		27
	3.2 Summary of Experimental Results		ary of Experimental Results	27
		3.2.1	Powder Feedstock Characterization	27
		3.2.2	Fused Filament Fabrication Process Development and Sensitivity	28
		3.2.3	Sustainability and Scalability	30
	3.3	Conclu	sion and Recommendations on FFF Evaluation	32
4.0	Shear Assisted Processing and Extrusion Tube Forming			34
	4.1	Work scope		34
	4.2	Background on ShAPE		35
	4.3	3 PM2000 ShAPE Manufactured Tube		36
		4.3.1	Fabrication	36
		4.3.2	Characterization	37
	4.4	ShAPE	Manufactured 14YWT ODS Steel	40
	4.5		sions and Recommendations on Feasibility Study on ShAPE Tube	42

Contents

5.0	Feasibility Study Conclusions and Recommendations		44
	5.1	Conclusions and Recommendations on Cold Spray and Additive Friction Surfacing	44
	5.2	Conclusion and Recommendations on FFF Evaluation	44
	5.3	Conclusions and Recommendations on ShAPE Evaluation	45
6.0	Application Space for Solid-State Processing in the Nuclear Industry		47
7.0	Refe	ences	49

Contents

Figures

Figure 1.	Schematic of the solid-state manufacturing processes feasibility study and process development phases	
Figure 2.	Field portable high-pressure cold spray diagram	
Figure 3.	Electron backscatter diffraction of cold sprayed nickel-yttria (Gwalani et al. 2022)	
Figure 4.	 (a) FSP repair of simulated chloride-induced stress corrosion cracking in 1-inch-thick 304L SS coupons performed at Pacific Northwest National Laboratory (top). (b) EBSD micrograph highlighting the refined grains present in the FSP material (bottom) 	
Figure 5.	Optical micrographs of cold spray deposits. Left: cold spray of optimized 316L SS powder with less than 1% porosity. Right: cold spray of non-optimized 316H SS powder with 24.01% ±1.08% porosity	18
Figure 6.	Etched dark field optical micrograph of friction stir processed cold sprayed 314H SS material deposited onto a 316L SS substrate	19
Figure 7.	Etched dark field optical micrographs. Left: top micrograph location as indicated in Figure 6. Right: bottom micrograph location as indicated in Figure 6.	19
Figure 8.	SEM (left) and EDS (right) map of dark indications seen in etched micrographs of the bottom of the FSP region. EDS results suggest indications seen in optical microscopy (Figure 9) are boron-nitride particles from the PCBN FSP tool.	20
Figure 9.	Optical micrograph of HPCS+FSP sample with a red box indicating the region explored by EBSD shown in Figure 10	21
Figure 10.	An EBSD montage showing the grain size of the HPCS+FSP material. (a) EBSD of the strip shown in Figure 9. The black boxes define the bottom top and middle areas of examination. (b) and (e) are higher magnification images of the bottom area of examination. (c) and (f) are higher magnification images of the middle area of examination. (d) and (g) are higher magnification images of the top area of examination.	21
Figure 11.	EBSD inverse pole figures for bottom middle and top areas of examination, as defined in Figure 10, from left to right show a strong texture in the 101 direction that is a function of depth.	
Figure 12.	Pictures of the additive friction surfacing process (left) and the processed sample showing locations for microscopy samples (right)	23
Figure 13.	Optical micrograph showing the etched transverse cross-section of the AFS sample.	23
Figure 14.	Hardness map of the AFS sample showing a substantial increase in strength in the deposited material compared to the substrate	24
Figure 15.	EBSD images at various positions throughout the AFS sample height	24
Figure 16.	Optical micrograph	
Figure 17.	An EBSD montage of the FSW build showing the grain size of the HPCS+FSP material. (a) EBSD of the strip shown in Figure 16. The black boxes define the top, middle bottom areas of examination from left to	

Figures

	examination. (c) and (f) are higher magnification images of the middle area of examination. (d) and (g) are higher magnification images of the top area of examination.	25
Figure 18.	Schematic of the FFF process	27
Figure 19.	SEM images of 14YWT ODS Batch 1 and 316H as received powder, A and C. Optical microscopy of as received 14YWT ODS Batch 2 as received powder, B.	28
Figure 20.	Particle size distribution of as received ORNL ODS powder Batch 2 and 316H stainless steel	28
Figure 21.	Filament loading 65% by volume fabricated from 14YWT 325 mesh spherical powder	29
Figure 22.	First components printed by the 65% vol 14YWT ODS filament (with binder)	30
Figure 23.	Images of green print pieces produced from 316H SS batch 2 powder	30
Figure 24.	Image analysis at edge of as-fabricated 316H SS (Print #6)-Flat Cube (red box). Observations at various magnifications using backscatter (A1-A3) and secondary imaging modes (B1-B3)	31
Figure 25.	SEM micrographs of sintered 316H SS Print #6. Planar views (left) near left edge and (right) center of the sample and (bottom) cross-sectional images. (a) and (b) show backscattered electron and secondary electron imaging mode images, respectively.	32
Figure 26.	Schematic of the billet forming processes applied for ODS ShAPE experiments	34
Figure 27.	(a) The ShAPE process uses shear to locally heat, consolidate, and extrude materials. (b) The world's first dedicated ShAPE machine at PNNL	35
Figure 28.	Photographs of extrusion tooling and materials	36
Figure 29.	Image showing (a) the PM2000 tube extruded via the ShAPE process, (b) its cross section showing that the extrudate is a tube for the most part, and (c) vertical indirect extrusion process output	37
Figure 30.	SEM micrographs comparing PM2000 steel microstructure in (a) as- received condition and (b) following ShAPE tube processing, demonstrating the evolution of grain structure and oxide particle distribution during thermomechanical processing	
Figure 31.	PM2000 base metal (rod) and ShAPE tube samples. (a) Precipitate size distribution and (b) average precipitate size and density distributions. BM, S-Start, S-Middle, and S-End denote base metal, start, middle, and end sections of the ShAPE tube.	39
Figure 32.	Vickers microhardness profile of PM2000 base metal rod. (a) Longitudinal sample; (b) transverse sample and ShAPE extruded samples in longitudinal direction: (c) start, (d) middle, (e) end, and (f) ShAPE extruded middle sample in transverse direction. Note that the color map shows the hardness in HV, while X and Y axes denote distance in	
	millimeters	39

Figures

Figure 33.	Summary of ShAPE process input and output for the four experiments completed for ODS steels	
Figure 34.	Comparative extruded images of the PM2000 and 14YWT SPS starting	
	material	41

Figures

Tables

Table 1.	HPCS machine parameters used	18
Table 2.	FSP parameters for FSP of HPCS 316H material	18
Table 3.	Filament composition	29
Table 4.	Applications space and benefits for solid-state manufacturing processes	48

Tables

1.0 Introduction

The Advanced Materials and Manufacturing Technologies (AMMT) program develops crosscutting technologies in support of a broad range of nuclear reactor technologies and maintains U.S. leadership in materials and manufacturing technologies for nuclear energy applications. The overarching vision of the AMMT program is to accelerate the development, qualification, demonstration, and deployment of advanced materials and manufacturing technologies to enable reliable and economical nuclear energy (Li et.al. 2022)

The AMMT program will exploit additive manufacturing (AM) to develop and optimize reactor materials and introduce new high-performance materials into nuclear energy systems. AM is an innovative technique to produce components at near-net shape with minimal machining. In some cases, the typical engineering alloys are not well suited to be produced through AM. Therefore, the AMMT program is further exploring other optimized alloy/manufacturing combinations for improved performance like increased radiation tolerance but also improved high-temperature strength, creep resistance, and environmental effects.

Solids-based AM techniques can overcome some of the challenges in liquid-based AM processes and should therefore be considered in material design and manufacturing as well. Solid-phase techniques may be better applicable to some materials and/or components than liquid-based techniques, for example, tube manufacturing. Solid-state AM techniques generally are divided into two broad categories—plastic deformation-based and sinter-based—depending on metallurgical bonding mechanisms, range of processible alloys, and resulting microstructures (Tuncer and Bose 2020). Binder jetting uses a binder to hold powder together, followed by sintering that consolidates the powder into a dense part without melting. This technology may be well suited for producing complex parts of oxide dispersion strengthened (ODS) alloys. Other advanced manufacturing techniques use severe deformation to impart high densities of dislocations in the material while forming it into a tube or plate form (Azushima et.al. 2009). This does not allow one to produce complex shapes but can be used to form tube, plate, or rod materials with a high density of sinks for extreme radiation tolerance.

The work presented in this report represent a feasibility study on solid-based AM techniques of 316 stainless steels (SS) and ODS steel components and supports the vision and goals of the AMMT program relevant to accelerate development and deployment of advanced manufacturing processes. Achieving this can provide a safety improvement through larger safety margins, economic benefit for higher efficiency during operation

1.1 Project Objectives and Overview

The objectives of the solid-state manufacturing feasibility project are:

- Assess the benefits of solid-state advanced manufacturing processes for nuclear energy products. This work will provide feasibility information on alternative routes for ODS steel manufacturing.
- 2. Demonstrate the sensitivity on final microstructural and residual stresses from the powder microstructure and composition.

This overall project provides the U.S. Department of Energy (DOE) a critical feasibility study comparison of three solid-state processes to other AM processes, thereby providing the

Introduction 13

feasibility of the solid-state processes examined to manufacture 316H SS and ODS steel components (Figure 1):

- Fused-filament fabrication (FFF): This work provides an initial evaluation of the impact of powder morphology and sizes on the FFF process, and the feasibility and adaptability for different material systems, to use FFF for ODS steels and 316SS.
- Shear-assisted processing and extrusion (ShAPE): Specifically for this portion of the project
 on ShAPE tube forming, the objectives will be to determine the feasibility to direct tube
 forming of high tensile strength steel tubing, specifically for ODS steel to determine the
 effect of the patented extrusion process on the dispersoids of the ODS material.
 Additionally, as often ODS powders are mechanically alloyed and therefore more platelike
 or angular, this feasibility was to explore the impact on the optimization process and initial
 feasibility of direct tube forming.
- Cold spray (CS) and friction stir additive manufacturing (FSAM) as a stretch goal: Bulk
 and near net shape manufacturing processes for high temperature. High-strength alloys
 are needed. Additionally, CS techniques can be applied in situ at the operational level for
 repair and can provide multiple benefits to the nuclear industry. These tasks aim to provide
 information to show benefits of CS during the full life cycle, namely research and
 development (R&D), product manufacturing, and repair to mention a few key points.

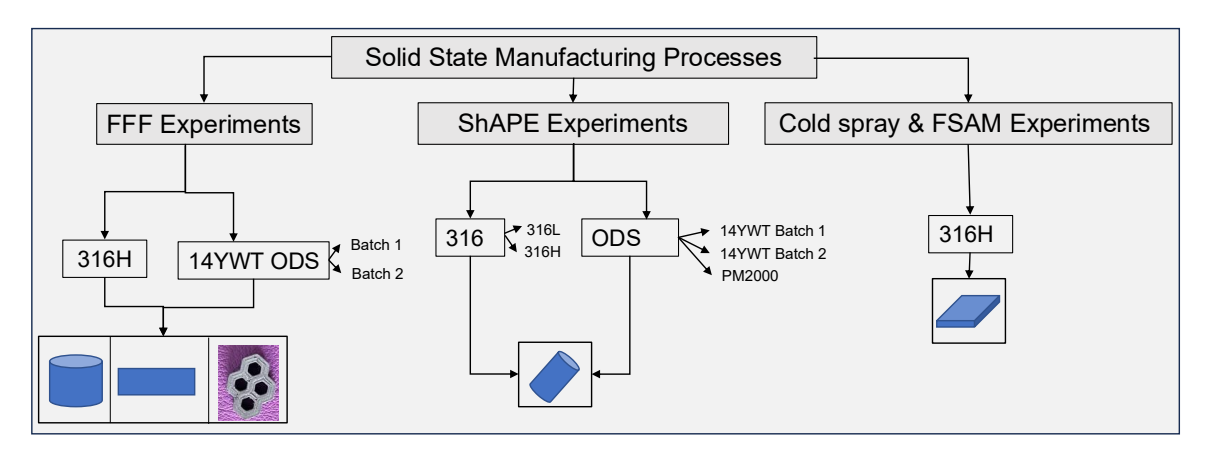


Figure 1. Schematic of the solid-state manufacturing processes feasibility study and process development phases

1.2 Work Scope

This report provides the results and preliminary feasibility study of three types of solid-state manufacturing methods for introduction and potential applications within the nuclear industry. The experimental work which explores the feasibility of CS and FSAM has not been reported previously and is therefore detailed and discussed in Section 2.0. Both the FFF and the ShAPE experiments were already previously detailed in separate milestone reports and therefore only a summary of each are provided in Sections 3.0 and 4.0. Conclusions are provided in Section 5.0 and in 6.0 the "Application Space for Solid State Processing in Nuclear Industry" is provided. This feasibility study does not make provision for full optimization and therefore structural comparisons between properties of each method, as well as quantitative benchmarking against wrought materials.

Introduction 14

2.0 Toward Additive Friction Surfacing of Stainless Steel 316-H for Large-Scale Additive Manufacturing

2.1 Iterative High Pressure Cold Spray and Friction Stir Processing

Iterative CS and friction stir processing (FSP) resulted in improved properties. Cold spray has many salient benefits compared to other deposition processes. High-pressure cold spray (HPCS) can achieve high-precision deposition of non-weldable materials with low porosity and also can enable local composition control. However, it is challenging to achieve full density in the bulk material, and interface strength can be a limiter to mechanical performance. Furthermore, the costs associated with use of helium gas and powder manufacturing can limit economic viability. Nitrogen gas is a cheaper carrier gas alternative, by nearly two orders of magnitude, but has a lower critical velocity compared to helium gas because nitrogen molecules are larger in size. Because the velocity term in kinetic energy is squared, significantly less kinetic energy is available for conversion to plastic deformation energy in CS particles in nitrogen carrier gas compared to helium carrier gas. FSP provides a pathway to consolidate porosity intrinsic to HPCS and porosity introduced from using a cheaper nitrogen carrier gas while simultaneously homogenizing microstructure and refining grain size. In addition, the vertical material mixing induced by the FSP tool can help to fragment the layer-to-layer interfaces and further enhance materials properties.

2.1.1 Cold Spray Process Description

CS is a solid-phase deposition process. Particles are accelerated to supersonic velocities before impacting a substrate. The impact energy is sufficient to plastically deform the material at the interface, resulting in a mechanical interlock and metallurgical bonding. Minimal substrate heating occurs, dimensional stability is maintained, and detrimental thermal effects (heat affected zone [HAZ], thermal stresses, dilution layer formation, etc.) are avoided. A process diagram for a portable high pressure cold spray is shown in Figure 2. It should be noted the stationary high-pressure systems both the powder injection and heating occur in the in the spray gun itself, whereas in portable systems heating and powder injection occur upstream. Additional discussion about cold spray equipment can be found elsewhere (Ross et al. 2021).

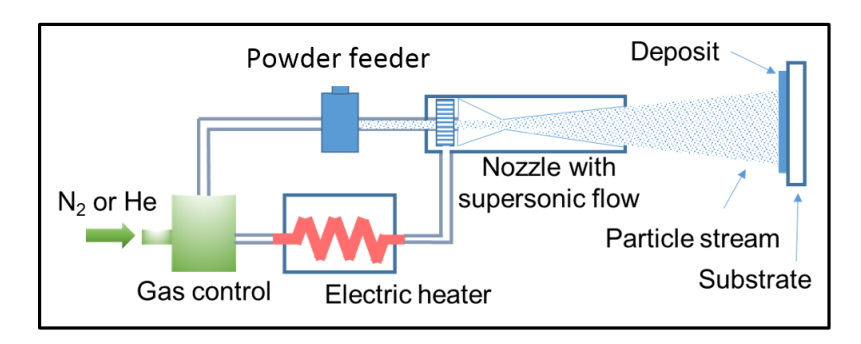


Figure 2. Field portable high-pressure cold spray diagram

HPCS is the metal cold spray process of greatest interest for high strength and high temperature metals and applications where improved properties are desirable. During HPCS, substrate heating is minimal, dimensional stability is maintained, and unwanted thermal effects (e.g., HAZ, thermal stresses, dilution layer formation, etc.) are avoided. <u>HPCS</u> systems operate at pressures typically ranging from 2–7 MPa (300–1,000 psi) and produce particle velocities

ranging from 800–1,400 m/s (Moridi et al. 2014). High velocity enables high kinetic energy, which is required to create high plastic deformation and shearing at particles boundaries. This results in dynamic recrystallization and metallurgical bonding at interparticle boundaries. Particles adhere to each other and to the substrate by both mechanical interlocking and metallurgical bonding. Figure 3 shows an electron backscatter diffraction micrograph of an HPCS nickel (Ni) alloy. This image is representative of excellent CS. Larger grains at the center of particles remain. Dynamic recrystallization exists on all particle boundaries. Which is indicative of good properties. In this particular image, black regions represent yttria rich particles or areas where grains are too fine to index (Gwalani et al. 2022).



Figure 3. Electron backscatter diffraction of cold sprayed nickel-yttria (Gwalani et al. 2022)

Low-pressure cold spray (LPCS) is of less interest because it fails to propel particles fast enough to achieve the kinetic energy needed for high-quality CS deposition of high melt temperature alloys. LPCS systems operate at 300 psi and lower. They typically produce particle velocities ranging from 300–600 m/s (Moridi et al. 2014). Reduced kinetic energy associated with LPCS means less plastic deformation, less interlocking, and no or dramatically reduced metallurgical bonding in high melt temperature materials (VRC Metal Systems 2020). Reduced kinetic energy means reduced mechanical properties. LPCS systems are not recommended for high-quality CS of steels, Inconel, and other high-strength/melt temperature materials.

2.1.2 Friction Stir Processing Process Description

Friction stir welding (FSW) is a solid-phase joining process and is achieved by spinning a non-consumable tool and plunging it into the workpiece. Frictional heating and material deformation enable the formation of a plasticized region below the tool shoulder called the stir zone. The FSW tool and stir zone are traversed across the joint, effectuating a weld. Temperatures generated during FSW are typically between 60% and 80% of the absolute melting temperature of the workpiece material. FSP is the use of FSW for purposes other than joining such as material property modification and repair. Use of FSP to repair chloride-induced stress corrosion cracking cracks is shown in Figure 4(a). FSP typically leads to microstructure homogenization and grain refinement. Figure 4(b) shows the EBSD map showing the refined grain microstructure that leads to overmatched mechanical properties in the processed zone.

(a)

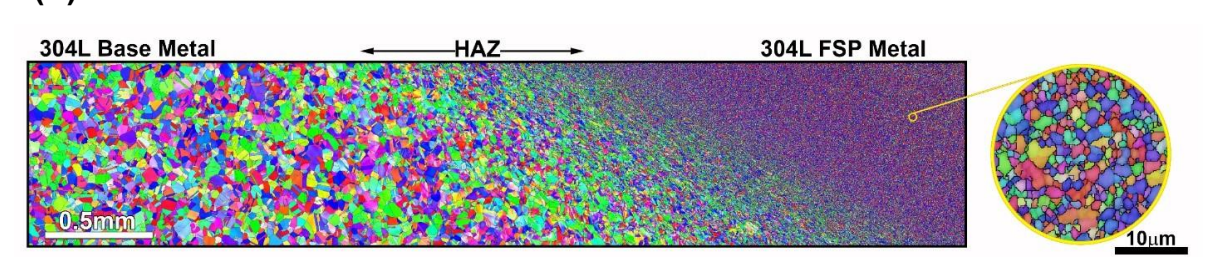


Figure 4. (a) FSP repair of simulated chloride-induced stress corrosion cracking in 1-inch-thick 304L SS coupons performed at Pacific Northwest National Laboratory (top). (b) EBSD micrograph highlighting the refined grains present in the FSP material (bottom)

Some advantages of FSW or processing are listed below.

- Temperature-controlled FSP ensures heat input is sufficiently low to avoid or reduce corrosion susceptibility in or around the weld.
- Initial results indicate the general corrosion resistance of the processed region is superior to that of arc welding and there is no detrimental HAZ
- Mechanical properties can be overmatched in austenitic stainless steels.
- It fully repairs physical defects (cracks, pitting) and microstructural damage (sensitization). It is a green process (i.e., no harmful fumes are generated, energy consumption is low).
- Weld or repairs can be done in a single pass.
- FSP is fully automated.

(b)

2.1.3 Experimental Method

316-H SS powder falls under Praxair product code "FE-445-C63." The certificate of analysis and certificate of conformability from Praxair report the following power size distributions, measurement per ASTM B822 (ASTM 2020), for the powder used in this work: D10, 51.5µm; D50, 72.5µm; and d90, 109.1 µm. Typically, optimal powder size range for CS equipment is 15 µm–40 µm. Powder is typically sieved and annealed to reduce variance from the optimal

diameter and increase particle ductility. Because of the lack of available powder and exploration nature of this task, the 316H SS powder was sprayed as received.

HPCS was done using PNNL's VRC Gen III Max CS using the parameters shown in Table 1. A 101 mm by 609 mm area was sprayed to a thickness of 4.17 mm. The substrate material is 316L SS plate. The substrate was cleaned with scotch bright wiped with isopropyl alcohol prior to cold spray. The first pass was run with the nozzle tilted °60 relative from the plate away from the direction of travel to enhance adhesion. The subsequent nine passes were sprayed with the nozzle perpendicular to the plate.

Carrier Carrier Gas Powder Feeder Travel Powder Feeder Carrier Standoff **VRC Nozzle** Gas Temperature Rotation Speed **Gas Flow Rate** Pressure Gas Model # (mm) Speed (RPM) (SLM) (°C) (mm/s) (psi) 650 6 200 .0060 200 900 Nitrogen 25

Table 1. HPCS machine parameters used

It should be noted that the larger powder diameter did not flow using standard parameters. The powder feeder rotation rate decreased, and the powder feeder flow rate was significantly increased to enable flow of larger particle sizes.

FSP was performed using PNNL's TTI FSW machine with PNNL's temperature control algorithms. FSP was done using the parameters shown in Table 2. A Mazak MegaStir tool made of polycrystalline cubic boron nitride (PCBN) with 30 wt.% W-Re tool. The tool geometry is convex scrolled step spiral (CS4) and is defined by model number E44230.

Table 2. FSP parameters for FSP of HPCS 316H material

Temperature Control Setpoint	Traverse Speed	Forge Force	Tilt
750°	25.4 mm/min	48.9 kN	0°

2.1.4 Results

An optical micrograph of 316H SS powder deposited by HPCS onto a 316L SS substrate is shown in Figure 5 with the optimized and non-optimized powders and processes.

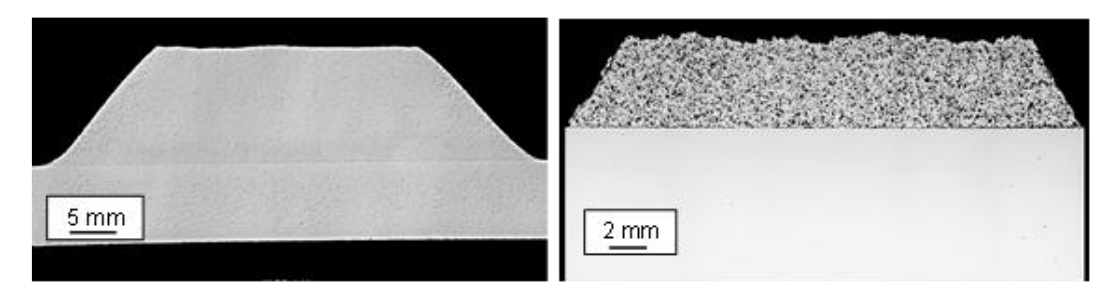


Figure 5. Optical micrographs of cold spray deposits. Left: cold spray of optimized 316L SS powder with less than 1% porosity. Right: cold spray of non-optimized 316H SS powder with 24.01% ±1.08% porosity.

In the optimized condition, there is less than 1% porosity whereas the non-optimized condition has ~24% porosity and a much rougher surface finish. The optimized cold spray of 316L SS

used powder sieved to create a tight size distribution near the experimentally determined optimum. The optimized process also uses helium gas. The non-optimized 316-H SS powder has a median particle size that is significantly larger than the known optimum and has a large variance in powder size. Nitrogen was used as the carrier gas. The combination of larger powder particle size and slower critical velocity of the carrier gas results in a significant reduction in the volume of material in particles that plasticize particles. This results in reduced interparticle bonding and higher porosity comparted to optimized processes.

An optical micrograph of the HPCS+FSP material is shown in Figure 6. No porosity exists in the FSP region outlined by the dashed green lines. Porous material can be seen in the cold sprayed region around the FSP region pointed out by the red arrows. The FSP tooling and processed region extended into the 316L SS substrate. Vertical mixing results in 316H SS being pushed into the 316L SS substrate and 316L SS being pulled into the HPCS+FSP region. The 316L SS appears lighter in the etched micrographs. Vertical mixing can be avoided with a different pin geometry on the PCBN FSW tool that uses flats instead of stepped spirals.

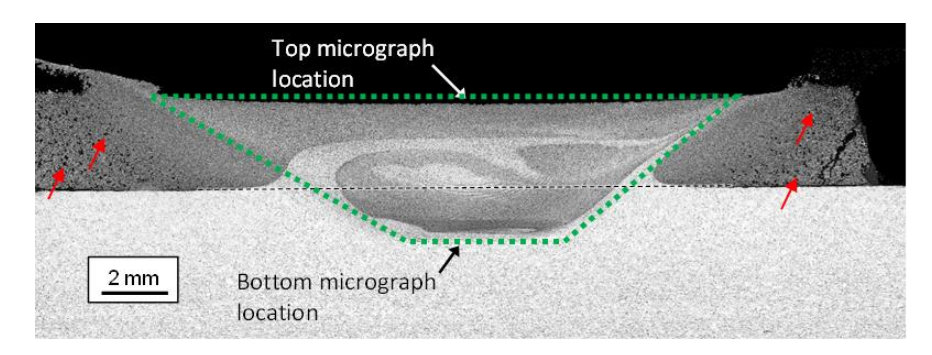


Figure 6. Etched dark field optical micrograph of friction stir processed cold sprayed 314H SS material deposited onto a 316L SS substrate

Micrographs of the top and the bottom of the FSP region are shown in Figure 7.

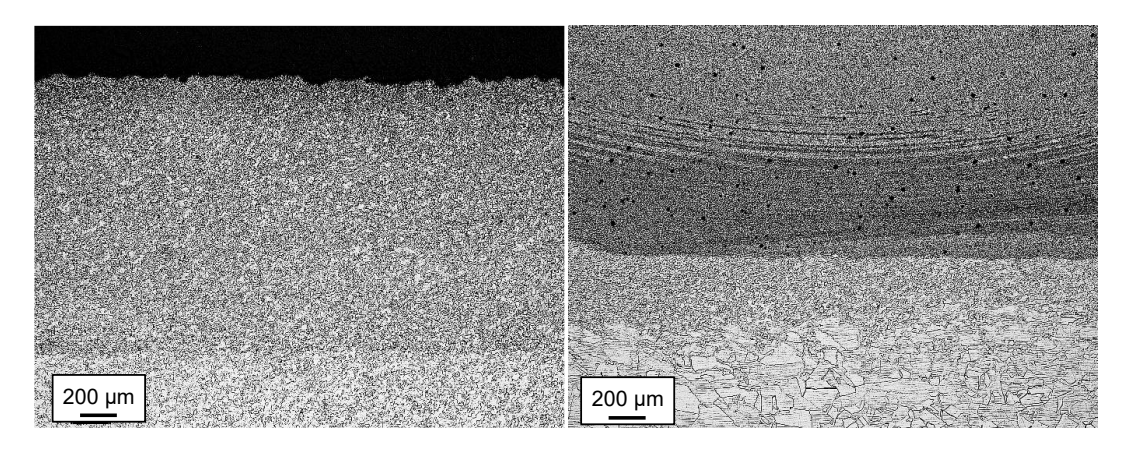


Figure 7. Etched dark field optical micrographs. Left: top micrograph location as indicated in Figure 6. Right: bottom micrograph location as indicated in Figure 6.

The top of the FSP region appears to be fully dense and ultrafine grained. The bottom of the FSP region shows dark indications that were not visible at lower magnification. Note that the size of these indications (4–5 μ m) is substantially smaller than the observed pores in the HPCS material (~50–100 μ m). Additionally, the thermos-mechanically affected zone and substrate

material just below the FSP region are entirely free of these indications. To better understand the nature of these indications, further microstructure characterization was performed near the bottom of the processed region.

Scanning electron microscopy (SEM) and energy dispersive spectroscopy (EDS) images are shown in Figure 8 for a region near the bottom of the processed region with several indications present. The lower magnification imaging (a) shows that the large-scale indications correspond to boron and nitrogen saturation. The tool used for FSP is made primarily of a polycrystalline boron nitride which suggests that these indications are a result of tool wear. The higher magnification image (b) shows the distortion field around the boron-nitride particle. Additionally, the small-scale circular indications correspond to chromium bright spots on the EDS mapping suggesting that these are nm scale precipitates rather than pores. PNNL has been advancing the state for the art for FSP of austenitic steels for many years and has never seen such a heavy concentration of boron nitride particles in the FSP region. Tool wear is usually more gradual resulting in trace amounts of contamination through the weld length. Alternatively, the failure can be catastrophic resulting in immediate tool and weld failure. Additional work is recommended to determine why this occurred. It is possible that the boron-nitride deposits are the results of an imperfect PCBN sinter. Alternatively, the presence of porosity in the HPCS material may inhibit thermal flow and lead to insufficient heating at the pin tip during FSP, thus increasing local tool wear.

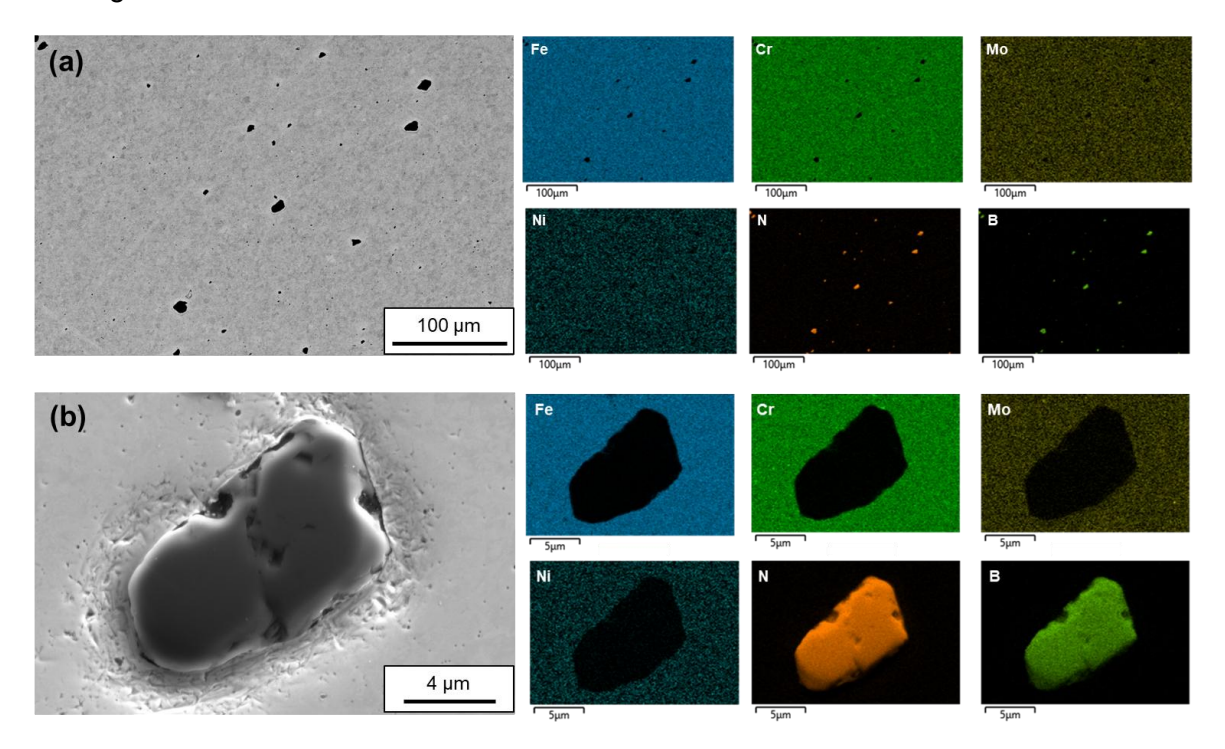


Figure 8. SEM (left) and EDS (right) map of dark indications seen in etched micrographs of the bottom of the FSP region. EDS results suggest indications seen in optical microscopy (Figure 9) are boron-nitride particles from the PCBN FSP tool.

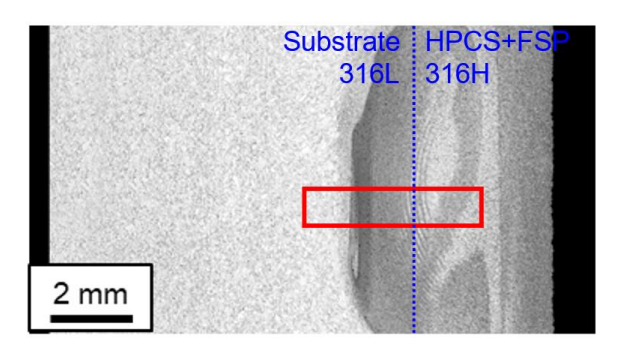


Figure 9. Optical micrograph of HPCS+FSP sample with a red box indicating the region explored by EBSD shown in Figure 10.

The EBSD montage shown in Figure 10 demonstrates the grain refinement from top to bottom of the HPCS+FSP region. The average grain size of the processed material is $2-4~\mu m$, which is notably smaller than the base material. The material at the bottom of the processed region generally has a lower grain size compared to the top of the processed region. This suggests that there may be an extreme temperature or strain gradient during processing. The grain size should be inversely proportional to the Zener-Holloman parameter. Higher strains/strain rates or lower temperatures will lead to reduced grain size.

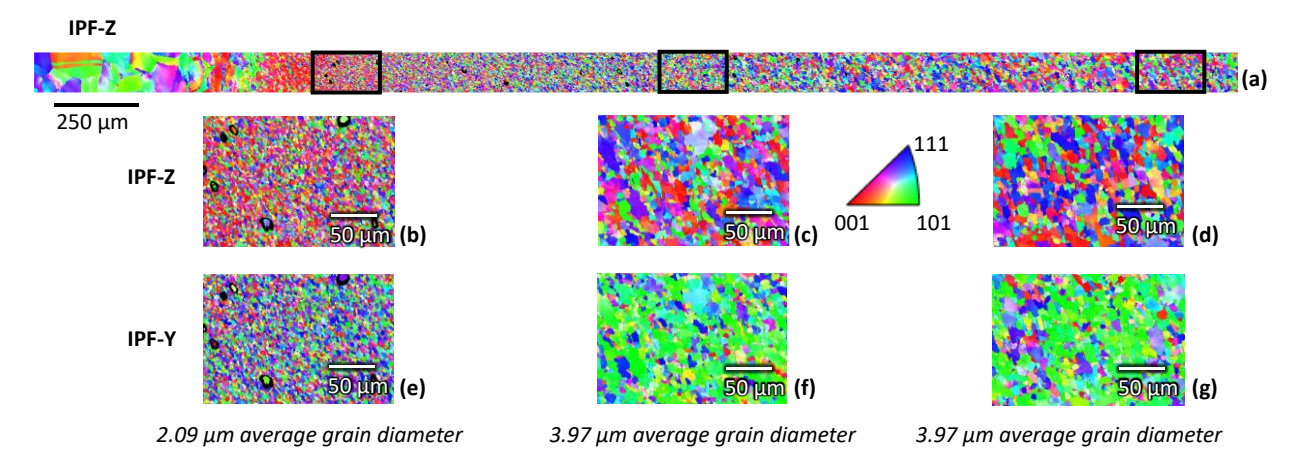


Figure 10. An EBSD montage showing the grain size of the HPCS+FSP material. (a) EBSD of the strip shown in Figure 9. The black boxes define the bottom top and middle areas of examination. (b) and (e) are higher magnification images of the bottom area of examination. (c) and (f) are higher magnification images of the middle area of examination. (d) and (g) are higher magnification images of the top area of examination.

Additionally, the EBSD inverse pole figures, Figure 11, show a strong texture along the 101 directions as a function of depth. The highest texturing occurs near the center of the processed region. Additional characterization would be needed to understand if the texturing is a result of the HPCS-substrate interface or if it is a result of an FSP processing history gradient.

Figure 11. EBSD inverse pole figures for bottom middle and top areas of examination, as defined in Figure 10, from left to right show a strong texture in the 101 direction that is a function of depth.

2.2 Additive Friction Surfacing

Previous work shows that low-temperature FSW or processing of austenitic stainless steels can produce material with overmatched mechanical properties and equivalent general corrosion performance relative to the base metal with no detrimental HAZ (Ross and Alabi 2019; Bhattacharyya et al. 2021). Advances in process control from friction stir based processes can produce repeatable ultrafine grain structure, and therefore properties, despite the presence of process disturbances. FSAM techniques have the potential to produce near-net shape parts with overmatched bulk properties, compared to extruded plate or forgings, similar to that produced by low-temperature FSW or processing.

2.2.1 Additive Friction Surfacing Process Description

Additive friction surfacing (AFS) is a FSAM technique that is effectuated by spinning a consumable metal rod or bar stock, applying a forge force, and traversing along a build path. The primary differentiator of AFS compared to other FSAM techniques is that AFS does not use a consumable tool; rather, it only uses the feedstock for deposition. Consumable tooling required for FSAM techniques such as additive friction stir deposition of SS are made from materials such as, especially PCBN composites and tungsten rhenium, which are cost prohibitive for large scale additive manufacturing (LSAM) for stainless steels. Until a significant breakthrough is made in tool material for processing stainless steels, all FSAM process requiring consumable tooling are anticipated to be cost prohibitive for LSAM of stainless steels. In contrast AFS uses rod stock, which is typically less than one third the cost of weld wire. This means that AFS has the potential to outcompete melt-based processes on cost for near net shape (NNS) LSAM.

Figure 12 shows the AFS of the 316H SS build studied in this work. It is plainly seen that there is no consumable tooling. The spinning 316H SS rod is pressed against the substrate and traversed along the build path. This first attempt for AFS of 316H SS is approximately 12 mm x 75 mm x 50 mm and is free from volumetric defects.



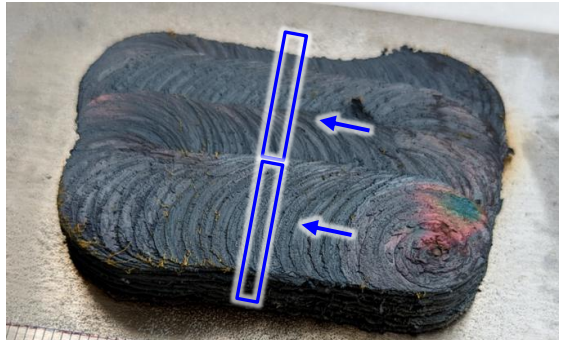


Figure 12. Pictures of the additive friction surfacing process (left) and the processed sample showing locations for microscopy samples (right)

2.2.2 Experimental Procedures

This work demonstrates feasibility of AFS for NNS LSAM. The first attempt build is approximately \sim 12 mm x 75 mm x 50 mm. The feedstock used for this build is 25.4 mm 316-H SS rod. The deposition was run at 500 RPM, 35 kN, 400 mm/min traverse rate and no tilt. Overlap between passes was 30% of the rod diameter. Deposits were performed on a 12.7-mm thick 304L SS plate.

Analysis using ASTM Standard E384-22 (ASTM 2022) was performed using 300 gf and 12 s dwell time with a spacing of 0.2 mm. Optical microscopy (OM) of the etched cross sections is shown in Figure 13. The OM image indicates that the build is free from volumetric defects. Oxidation at vertical layer boundaries is visible in OM image and verified using EDS. Cross sections were cut at the locations shown in the Figure 12. Interfaces between adjacent layers (horizontal passes) were not detectible via optical or electron microscopy. This indicates excellent horizontal mixing at 30% overlap.

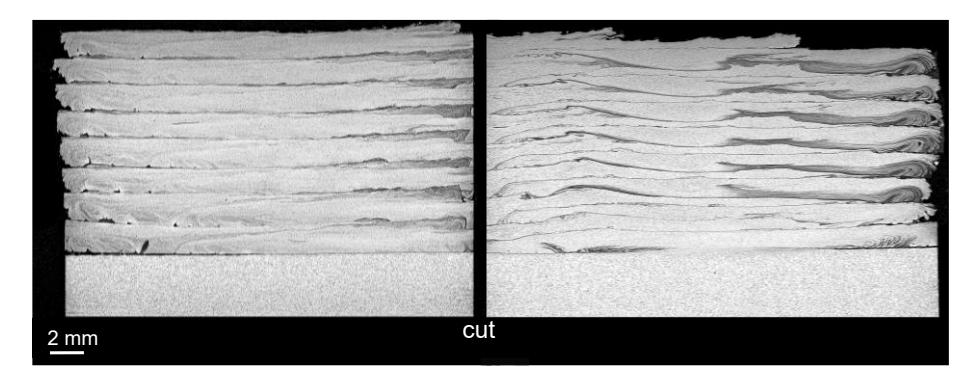


Figure 13. Optical micrograph showing the etched transverse cross-section of the AFS sample.

Hardness results for an area with a slight offset from the sample center are shown in Figure 14. Note that the bulk of the processed material has a hardness ~240 HV compared to the base hardness <200 HV. There are some higher hardness regions ~280 HV that correspond to oxides at the layer-to-layer interfaces. Additionally, the very top of the region has a slightly lower hardness compared to the bulk. This suggests that the reheating effect from subsequent layer deposition leads to a change in phase morphology with a positive influence on mechanical properties.

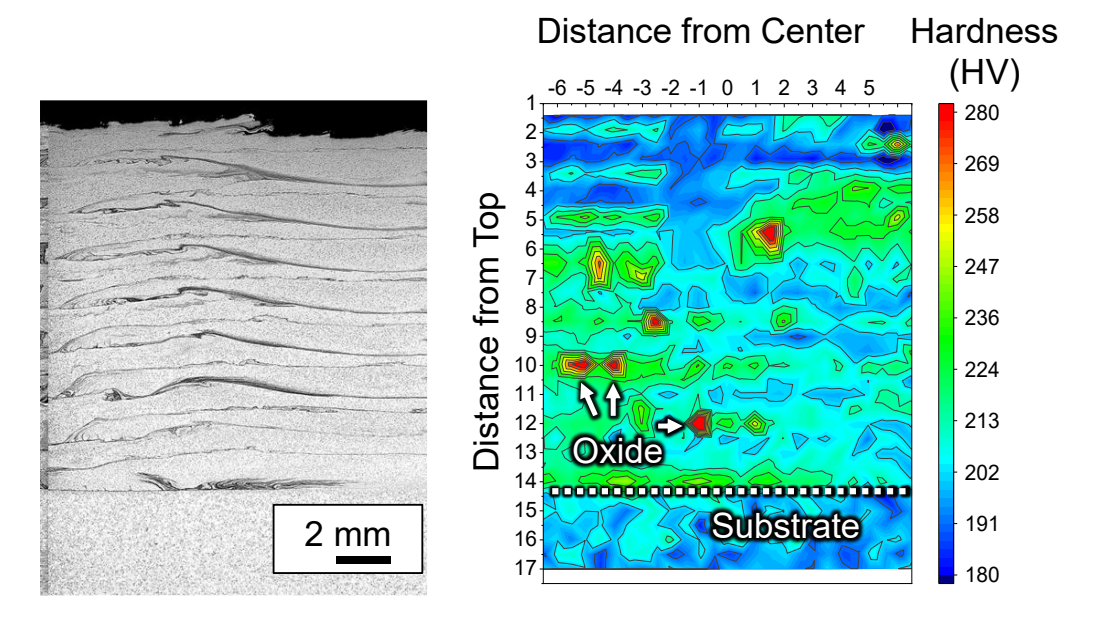


Figure 14. Hardness map of the AFS sample showing a substantial increase in strength in the deposited material compared to the substrate.

EBSD scans were done at various locations throughout the build as indicated in Figure 15. For the scanned regions, the average grain size varied from 4.0 to 6.8µm.

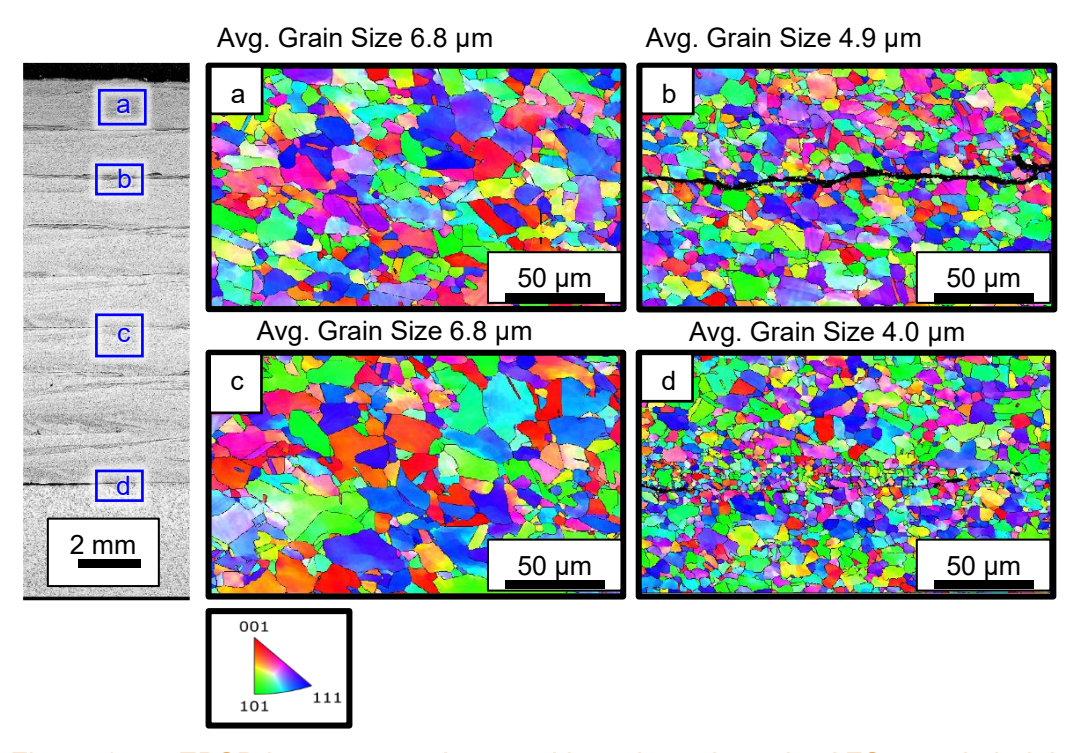


Figure 15. EBSD images at various positions throughout the AFS sample height

This is approximately one-fourth the average grain size of the extruded plate and approximately an order of magnitude reduction compared to forging specifications (assuming 6–4 max ASTM#) for 316H SS. Region (a) represents the center of the topmost layer deposited. Regions (b), (d), and (d) represent vertical interfaces with d being the interface between the substrate and the first deposited layer. Regions (b) and (d) show that grains are further refined near the interlayer boundary. Region (c) shows an interface where the interlayer boundary is not readily apparent, grain size is homogenous and comparable to region (a). OM shows that the lower half of the build appears to have better vertical mixing at the interface. Interfaces are hard to detect and oxides that exist at the interface appear to be mixed into the layers appearing as swirls that indicate flow patterns. The OM image and An EBSD montage of the FSW build showing the grain size of the HPCS+FSP material are shown in Figure 16 and Figure 17, respectively.

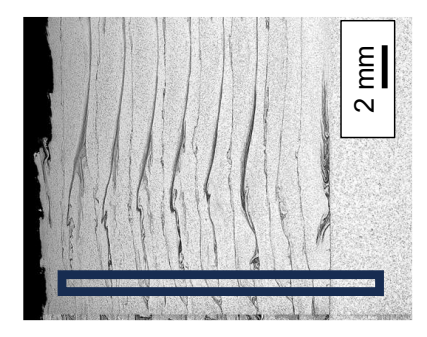


Figure 16. Optical micrograph

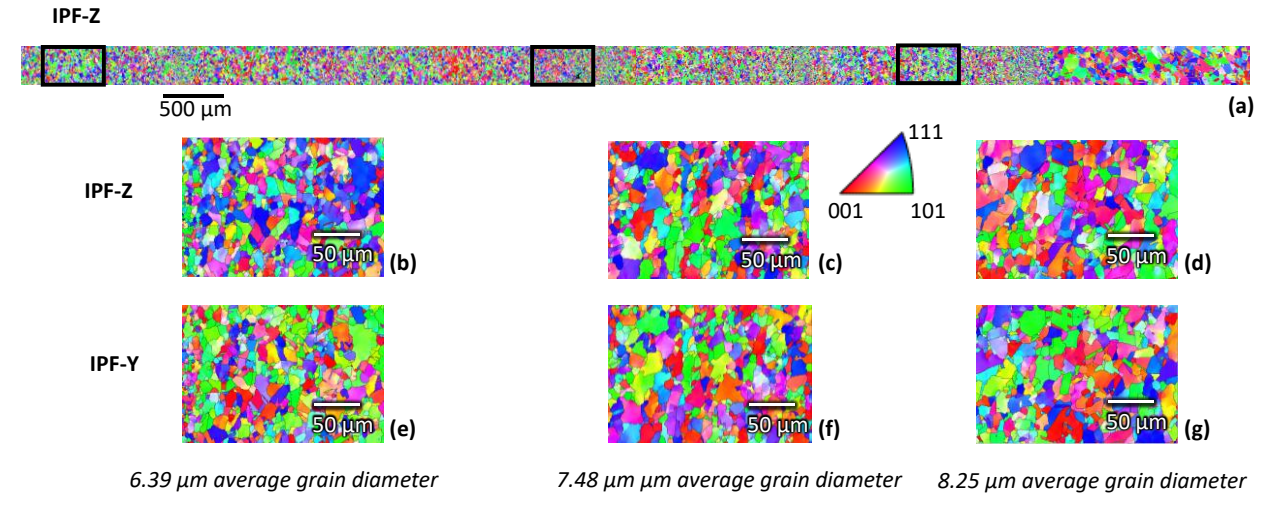


Figure 17. An EBSD montage of the FSW build showing the grain size of the HPCS+FSP material. (a) EBSD of the strip shown in Figure 16. The black boxes define the top, middle bottom areas of examination from left to right. (b) and (e) are higher magnification images of the bottom area of examination. (c) and (f) are higher magnification images of the middle area of examination. (d) and (g) are higher magnification images of the top area of examination.

These results suggest that additional processes development and improved process control can produce builds that have sufficient vertical and horizontal mixing to produce fine grained homogenous microstructures, and therefore properties, throughout the build. Work performed in a separate program has demonstrated that an argon atmosphere can greatly reduce the formation of oxides at these interfaces. Additional tuning of the process parameters can be sufficient to break up oxides and enhance vertical mixing.

The existing grains are approximately 4–6 times larger than those reported for LTFS processing (Jiang et al. 2019; Bhattacharyya et al. 2021; Garcia et al. 2024). Further process development can further reduce grain size to achieve associated increases in mechanical properties and corrosion performance. We anticipate this is achievable through improved process development and process controls. Deposition rate for the sample in this work is approximately 9 kg/hour. We anticipate with proper development this process can approach and possibly exceed 45 kg/hour per deposition head.

2.3 Conclusions and recommendations on Cold Spray and Additive Friction Surfacing

The initial CS experiments using 316H SS powder size (similar to laser powder directed energy deposition powder) were not sufficient to provide a fully bonded structure. However, alternating CS with FSP resulted in an inherent bonded and dense structure.

- Equiaxed ultrafine grain structure produces improved properties and corrosion resistance
- Potential economic cost cladding or local AM
- Amenable to solid-phase alloying and functionally gradient chemistries/microstructures
- First attempt reduced grain size from ~27 to ~2–4 μ m. We anticipate ~1–1.5 μ m is achievable with process optimization.
- Boron-nitride particles from the PCBN FSP tool were unexpected and may indicate the tool is faulty and are not expected in future runs.

Significant technology developed is required to prepare AFS for commercialization; however, this work has demonstrated the following:

- AFS can create ultrafine grained builds of SS-316H using low-cost rod stock.
- Conditions exist in which interlayer boundaries are not readily visible, and grain structure is homogenous.
- Results show that AFS is a feasible method for NNS LSAM of nuclear components with improved properties and cost compared to competing techniques.

3.0 Preliminary Characterization and Evaluation on FFF Manufactured 316H and ODS Steels: Summary

This section is a summary of the technical report "Preliminary Characterization and evaluation on FFF Manufactured 316H and ODS Steels, PNNL-34985, September 2023, Carolyne A Burns, Saumyadeep Jana, Amrita Lall, Zachary C Kennedy, Michelle D Fenn, Joshua A Silverstein, Lorraine M Seymour, Isabella J van Rooyen" (Burns et al. 2023).

3.1 Background

This study seeks to evaluate FFF, a solid-state manufacturing technique, as an alternative method to laser-based AM. This section provides preliminary information on development of the FFF process using different powder types to demonstrate the sensitivity to powder morphology and size through the feasibility of manufacturing 316H SS and ODS steel components. A honeycomb structure and flat samples were targeted to demonstrate the flexibility of product form.

The FFF process is a filament extrusion-based AM method involving high-temperature sintering. Figure 18 shows a schematic of the various steps associated with the FFF process, which includes 1) filament fabrication, 2) three-dimensional shape printing, 3) binder removal, and 4) final high-temperature densification through sintering.

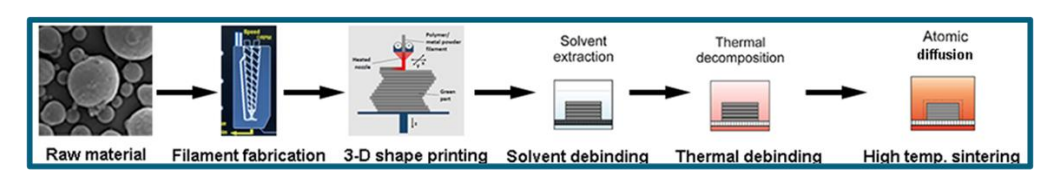


Figure 18. Schematic of the FFF process

3.2 Summary of Experimental Results

The FFF work scope included 1) two 14YWT ODS powder batches that provided information on the effect of different powder morphologies on the manufacturability with FFF and 2) two 316 SS powders to demonstrate the effect of powder size on the manufacturability using FFF. Powder morphology, particle size and particle size distribution, and flow properties were found to significantly affect extrusion for filament production and sintering outcomes.

3.2.1 Powder Feedstock Characterization

Images of the as received powders, 14YWT ODS Batch 1 with its large platelet particles, 14YWT ODS Batch 2 (obtained from Oak Ridge National Laboratory [ORNL]), small spherical particles, and the 316H SS powder that also has spherical particles are shown in Figure 19.

The platelet 14YWT ODS powder (batch 1) did not yield homogenous and high-density particle filament fabrication and prints regardless of the particle size distributions evaluated and the powder milling processes (cryo-milling and high-energy micro-milling). Both the 14YWT ODS batch 2 and the 316H SS powder, with their spherical morphology smaller particle size and tighter size distribution successfully produced printable filament. The size distribution of both materials is shown in Figure 20.

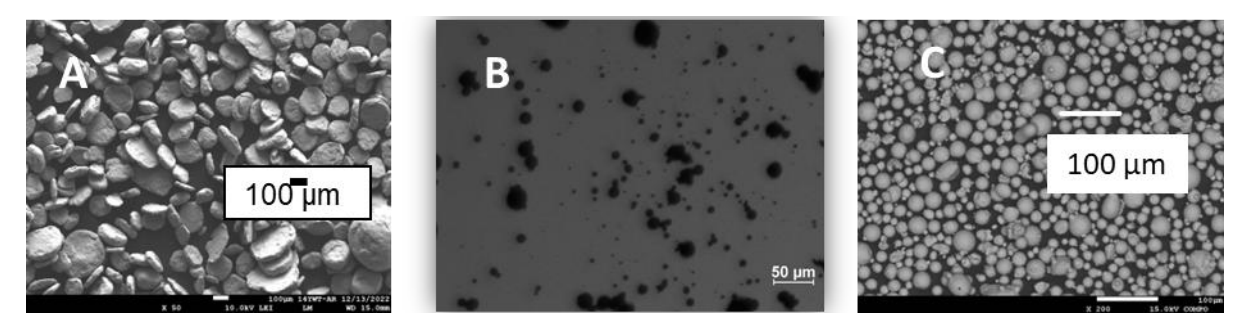


Figure 19. SEM images of 14YWT ODS Batch 1 and 316H as received powder, A and C. Optical microscopy of as received 14YWT ODS Batch 2 as received powder, B.

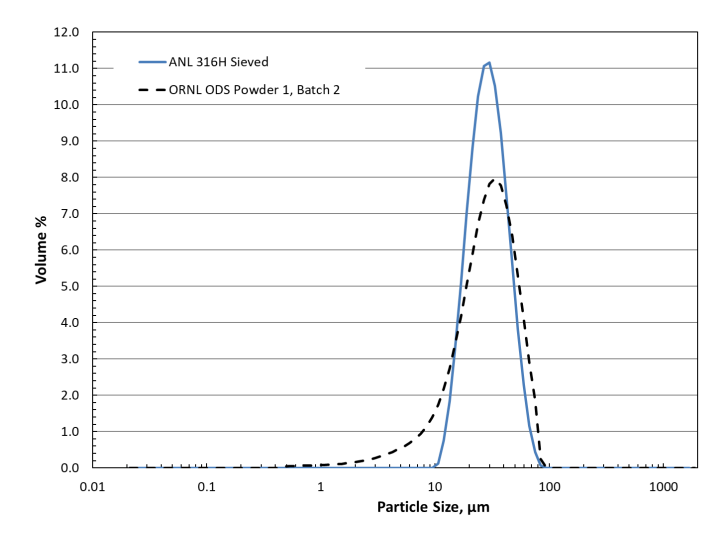


Figure 20. Particle size distribution of as received ORNL ODS powder Batch 2 and 316H stainless steel

3.2.2 Fused Filament Fabrication Process Development and Sensitivity

The FFF process involves several steps, including filament fabrication, shape printing, binder removal, and high-temperature densification. Through experimentation, sensitivities in filament fabrication, composition (Table 3) and printing were identified and related to:

- Powder particle morphology (size and shape).
- Powder loading percentages (65% for ODS steel, 62% for 316H SS).
- Binder efficacy during extrusion and sintering.

The powder content of the batch 2 ODS powder filament was successful at 65% by volume. The resultant filament was smooth and easy to handle with a diameter of 1.62–1.70 mm (Figure 21). The 65% vol. loaded filament was used to successfully print four components (Figure 22), namely three rectangular pieces (called flat cubes) and one honeycomb structure. The successful 316H SS batch 2 powder printed samples are shown in Figure 23. A custom built FFF printer was used for printing with a 0.4-mm SS nozzle, heated bed with a polyetherimide plate, a BondTech Extruder, and E3D heater block and heat sink. Repetier Host was used as the printer interface program, and a custom set of slicing parameters were set through the slicing software Slic3r.

Table 3. Filament composition

Component	ORNL ODS	316H
Binder	Volume %	Volume %
Polypropylene	25	27.1
Paraffin wax	8.3	9
Stearic acid	1.7	1.9
Metal Powder	Volume %	Volume %
316H	65	62
Material Type	Mass %	Mass %
Organic	6.3	6.4
Inorganic (316H)	93.7	93.6



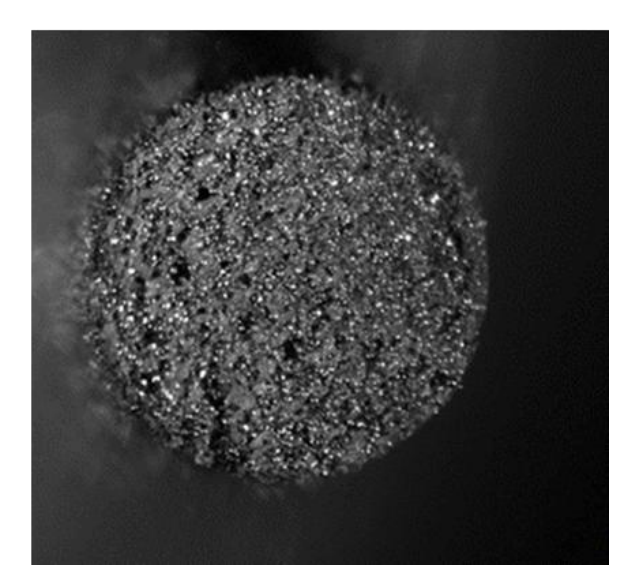


Figure 21. Filament loading 65% by volume fabricated from 14YWT 325 mesh spherical powder

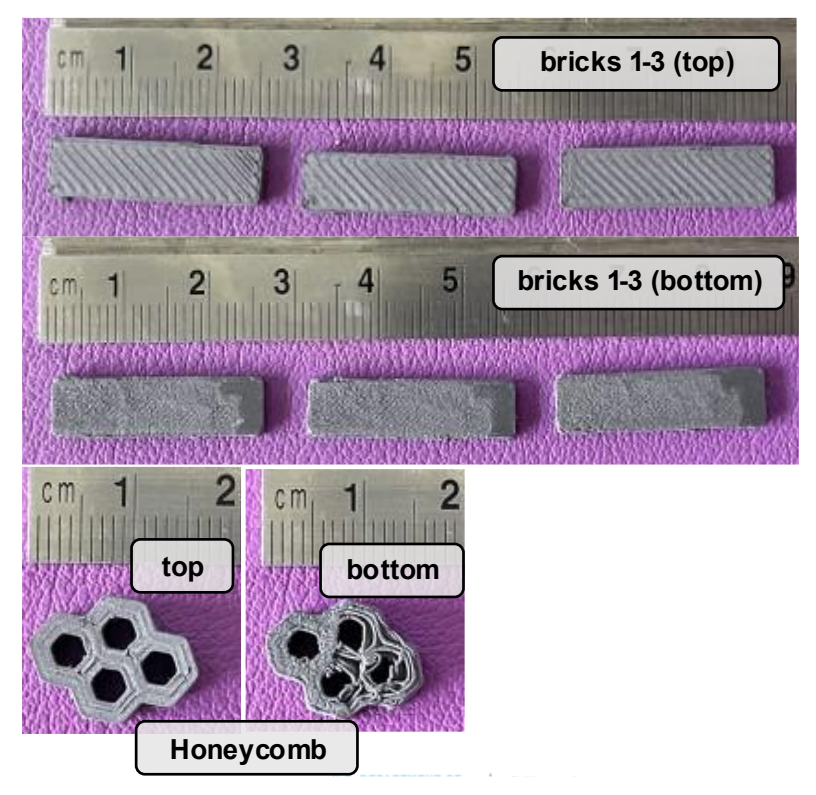


Figure 22. First components printed by the 65% vol 14YWT ODS filament (with binder)



Figure 23. Images of green print pieces produced from 316H SS batch 2 powder

3.2.3 Sustainability and Scalability

Subsequent sintering experiments confirmed successful densification, although additional optimization is necessary for structural integrity and density improvement. While both ODS steel and 316H components were successfully fabricated in the two geometrical forms, achieving higher-density parts through process scaling remains within the development domain and the scalability of FFF for industrial use will require further development.

The as-sintered surface characteristics of one of the printed forms are given in Figure 24 at various magnifications using backscatter (A1–A3) and secondary imaging modes (B1–B3). This provides information on the surface characteristics, topology, particle fusing, and gross void spaces. Figure 25 shows backscattered electron and secondary electron imaging SEM images near an edge and near the center of sintered 316H (Print #6) sample surface. The sample consisted of dense microstructure at both near edge and center regions of the sample, suggesting a considerably high sample density. Some pore characters are also observed in the sample, while they are only slightly lower at the center compared to the edge of the sample. The cross-sectional view of the sample also showed some pore character, while no significant difference between the sample surface or planar view and cross-sectional view is apparent. Spacing along interface of two depositional paths can also be observed in these SEM images.

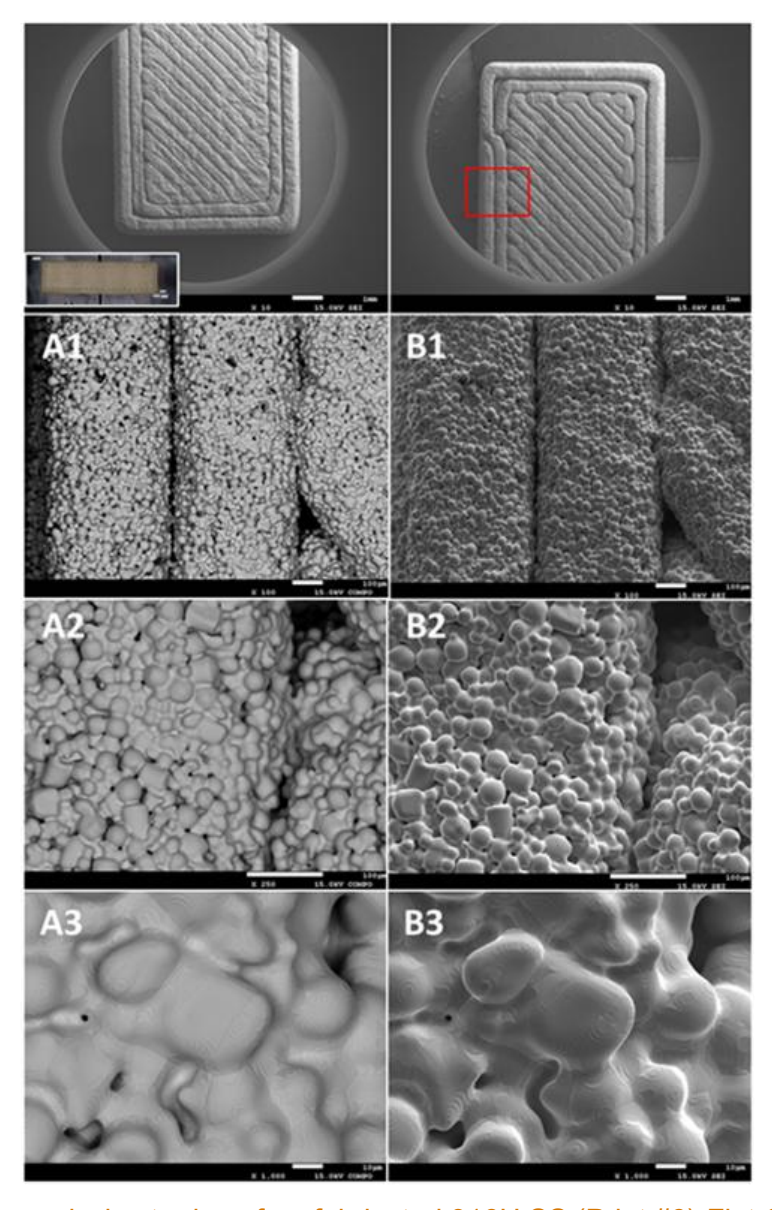


Figure 24. Image analysis at edge of as-fabricated 316H SS (Print #6)-Flat Cube (red box). Observations at various magnifications using backscatter (A1-A3) and secondary imaging modes (B1-B3).

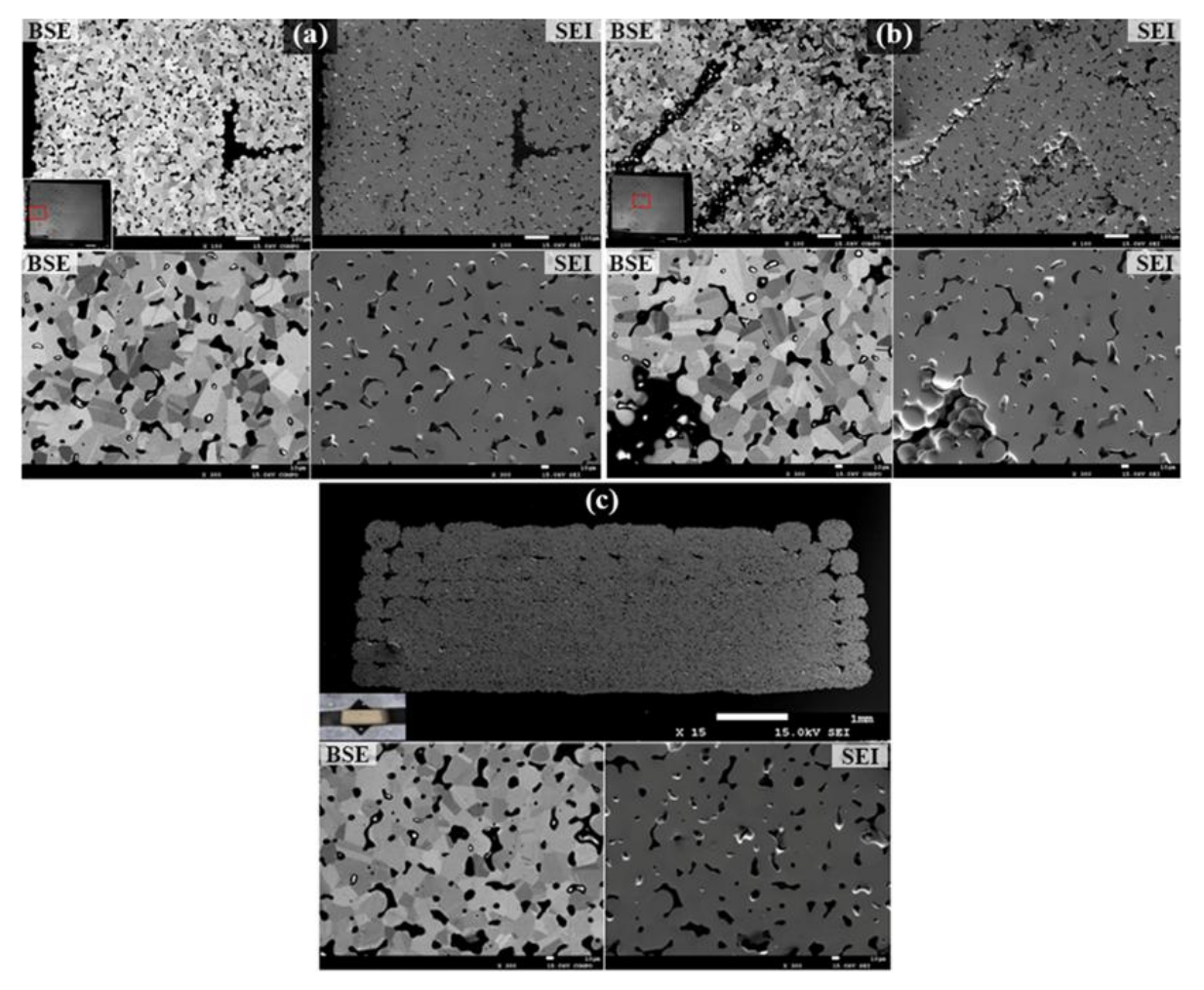


Figure 25. SEM micrographs of sintered 316H SS Print #6. Planar views (left) near left edge and (right) center of the sample and (bottom) cross-sectional images. (a) and (b) show backscattered electron and secondary electron imaging mode images, respectively.

3.3 Conclusion and Recommendations on FFF Evaluation

Feasibility of using FFF, a solid-state manufacturing technique, for fabricating parts from 316H SS and ODS steels was demonstrated by this work. Successful printing and sintering were achieved, with the following key takeaways:

- FFF provides superior control over microstructural features such as equiaxed grain size and oxide particle distribution compared to laser-based AM methods.
- Powder characterization plays an essential role in achieving manufacturable filaments and structurally sound components.
- While promising, optimization of sintering processes and scalability is required for full adoption in nuclear-grade applications.

The advancements described in the report hold significant promise for both nuclear energy systems and broader manufacturing applications. Impacts and applications are listed below:

Impact

- Safety Improvements: Enhanced microstructural control leads to higher mechanical strength and irradiation resistance, which is critical for reliable nuclear materials
- Economic Benefits: Reduction in waste and optimization of manufacturing processes result in lower production costs
- Sustainability: Solid-state AM methods minimize material waste by enabling near-net shapes from powder feedstock

Applications

- Nuclear Industry: Fabrication of nuclear grade components such as fuel cladding and structural elements for high-temperature reactors
- Aerospace Industry: Development of ODS steels with enhanced strength-to-weight ratios for space exploration
- Wider Manufacturing: Deployment in industries requiring precision-engineered parts, such as energy generation and automotive manufacturing.

It is recommended that the next phase of development include the following:

- Process improvements for achieving denser and larger components through the detailing on the particle size distribution window, as well as impurity levels to ensure structural integrity
- Customization of the polymer composition to increase the powder loading of the filament, and potentially the modeling of the process to accelerate the particle loading optimization
- Expanded applications of FFF techniques for complex geometries and critical reactor components
- Comparative studies across other solid-state techniques (e.g., CS, shear-assisted processing) to determine optimal manufacturing methods for various materials.

4.0 Shear Assisted Processing and Extrusion Tube Forming

This section is a summary of the following publications:

- Milestone report: Isabella van Rooyen, Mageshwari Komarasamy, Chinthaka Silva, Shalini Tripathi, Julian Atehortua, Mayor Pole, Tanvi Ajantiwalay, David Garcia, Quin R S Miller, Matthew Olszta, Ramprashad Prabhakaran, Tianhao Wang; "Preliminary Characterization and Evaluation on ShAPE Manufactured 316H and ODS Steels", M3CR-22PN0402023, PNNL-36737, September 2024, (Van Rooyen et al. 2024)
- Conference presentation: Silva, C.M., M. Komarasamy, J. D. Escobar, S. Tripathi, R. Prabhakaran, Q. R. S. Miller, T. A. Ajantiwalay, M. J. Olszta, I. J. van Rooyen. 2024a. A discussion on microstructural and mechanical characteristics of ShAPE extruded PM2000 FeCrAl tubes, TMS2024, March 3–7, 2024, Hyatt Regency Orlando, Orlando, Florida, USA (Silva et.al. 2024a)
- Journal publication: Chinthaka M Silva, Mageshwari Komarasamy, Julian D Escobar, Shalini Tripathi*, Ramprashad Prabhakaran, Quin R S Miller, Tanvi A Ajantiwalay, Matthew J Olszta, Isabella J Van Rooyen, "Manufacturing of oxide dispersion strengthened Fe-Cr-Al alloy using a nonconventional extrusion process", Accepted in JMEP, September 2025

4.1 Work scope

This section provides preliminary information on development of ShAPE forming for ODS steels only. The work on 316H SS was not performed as first. The feasibility study was performed on the two different ODS types for four experimental trials. Second, earlier work on 316L SS based on a PNNL Laboratory Directed Research and Development project has only recently been completed on wire ShAPE fabrication only and therefore did not provide sufficient resources and lessons learned to execute the tests as well. The planned work scope for the ShAPE study is shown in Figure 26.

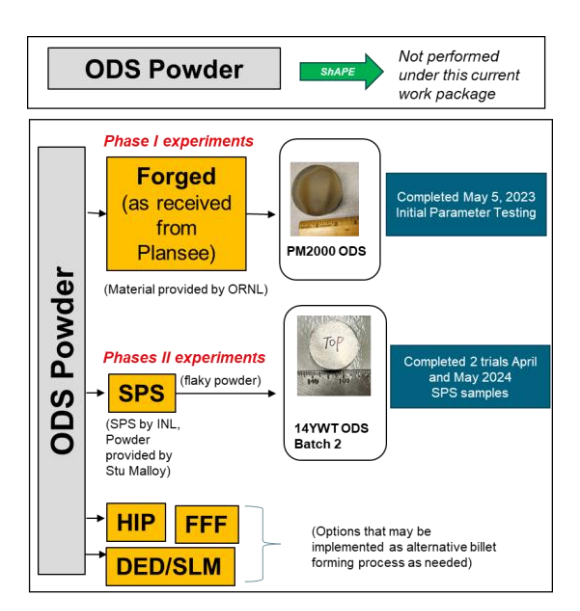


Figure 26. Schematic of the billet forming processes applied for ODS ShAPE experiments

4.2 Background on ShAPE

ShAPE is a solid phase processing technique that adds an additional shear force compared to conventional extrusion approaches (Figure 27.). Significant advantages of ShAPE are that it can be free from feedstock pre-consolidation and preheating, it is more energy-efficient, and it produces products with better strength, ductility, toughness, fatigue life, and surface finish. Research shows improved mechanical properties, fewer processing steps, and lower energy intensity through reduction or elimination of additional thermal processing (Whalen et al. 2021).

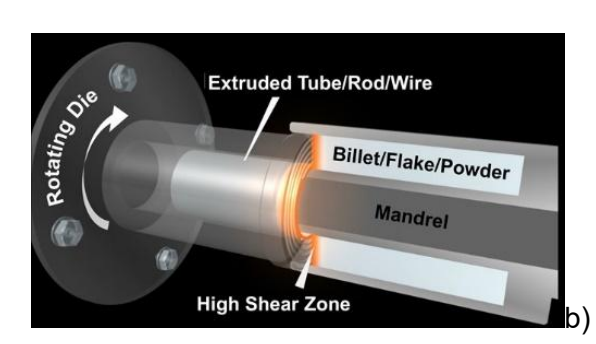




Figure 27. (a) The ShAPE process uses shear to locally heat, consolidate, and extrude materials. (b) The world's first dedicated ShAPE machine at PNNL.

In the ShAPE process, the interaction between the rotating die and the feedstock generates heat and severely deforms the feedstock material resulting in extreme microstructural refinement. Due to severe strain associated with the process, the interface between the clad and the core is metallurgically bonded with the formation of solid solution adjacent to the interface. Overall, extrusions produced via ShAPE (either clad or un-clad) typically exhibit improved performance compared to the conventionally extruded material. With PNNL's current ShAPE machine and direct extrusion tooling, a tube of 12 mm outer diameter and 0.5–1 mm wall thickness and rods of varying diameter can be fabricated from high temperature materials such as steels. With the ShAPE technology, various aluminum (Al) alloys, magnesium alloys, copper, nickel, and zircaloy tubes have been successfully fabricated. ODS steel rods also have been fabricated from Incoloy MA956 and CR-166 gas atomization reaction synthesized powders using the ShAPE technology (Zhang et al. 2022). Co-extrusion was successfully demonstrated via the ShAPE process on various alloys systems including co-extrusion of 7075 Al with 1100 Al, pure Cu with pure Ni, and Ni with Zircaloy-4 (Komarasamy et al. 2022).

To withstand the high temperatures and forces that will occur during extrusion, the die materials were carefully chosen and are shown in Figure 28. The key components that experience high temperature and processing forces during ShAPE extrusion are the extrusion die, container, and mandrel. In the current project, these components were designed and fabricated from high temperature materials. For instance, both the die and the mandrel will be made from W-La₂O₃ material. Additionally, the container that holds the feedstock will be fabricated from Inconel 718, a γ'' strengthened nickel base superalloy, which has the necessary high temperature strength, but most importantly, it is available in the size ranges that are required and is less expensive than MP159. Overall, the extrusion setup is well considered and designed and produces tubes from high temperature materials.



Figure 28. Photographs of extrusion tooling and materials

4.3 PM2000 ShAPE Manufactured Tube

The research results reported here in this section were a conference presentation (Silva et al. 2024a) and a detailed journal publication (Silva et al. 2024b).

4.3.1 Fabrication

The extruded tube and its cross section are presented in Figure 29a and Figure 29b with fabrication parameters shown in Figure 29(c). The die temperature was approximately 1,250°C at about the 2 mm plunge position. The temperature rise is due to frictional and adiabatic heating of the tooling and the billet material. The spindle torque was below 150 Nm and the ram force was below 40 kN for most of the extrusion. The rise at the end is due to the end of the billet, and the supposed deformation volume is interacting with the container base that is not deforming and is not at the steady-state temperature. Overall, the forces and torque were lower than expected; hence, the processing temperature can be reduced further to below 1,000°C to preserve the density of oxide dispersions for future similar material processing and optimization. After the processing, it was noted that the Inconel 718 mandrel had broken off during the extrusion process. This die failure can be mitigated by reducing the processing temperature and time, cooling the mandrel, and/or using tungsten-based mandrel material.

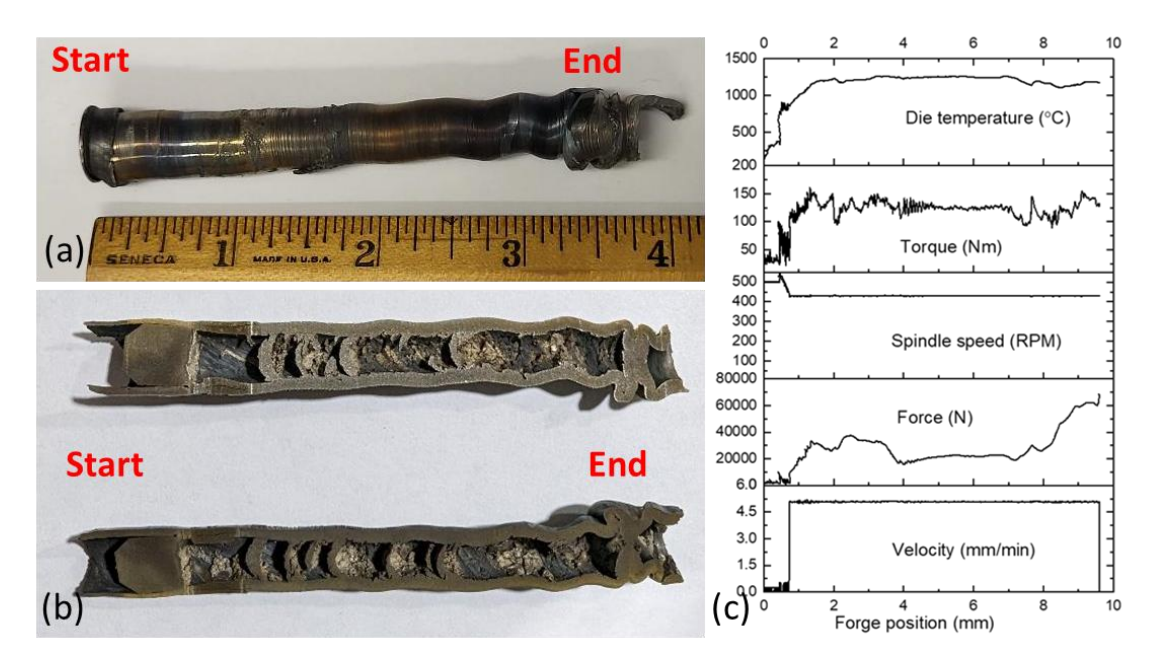


Figure 29. Image showing (a) the PM2000 tube extruded via the ShAPE process, (b) its cross section showing that the extrudate is a tube for the most part, and (c) vertical indirect extrusion process output

4.3.2 Characterization

XRD patterns of as-received (base metal PM2000) and ShAPE extruded tube (near the tube center) PM2000 samples showed only the presence of ferrous-based body-centered cubic ferritic structure with a space group of Im–3m. Rietveld refinement showed a smaller lattice parameter of the ShAPE samples compared to the as-received PM2000 alloy, but the decrease was only 0.04–0.07 % which is insignificant.

Microscopy analysis of as-received and ShAPE tube is presented in Figure 30(a) and Figure 30 (b), respectively. In the base metal, elongated grains along longitudinal and equiaxed along transverse directions were noted. Additionally, the presence of coarse secondary particles was noted. These were Al- and O-rich precipitates, and Y was also present in some parts of the precipitates, along with the presence of scattered Ti. Dispersoids in PM2000 steel consist of large oxides and nanosized oxide particles. Three nanosized oxide phases $Al_2Y_4O_9$, $Y_3Al_5O_{12}$, and $YAlO_3$ were noted in literature. In the ShAPE tube, presence of completely recrystallized equi-axed grain structure was noted. Average grain area was about 3.9 μ m² as compared to the base metal longitudinal section that exhibited 3.6 μ m². The presence of coarse dispersoids similar to the base metal were noted (Figure 30b(e)). These were primarily (Al,Y)O type and titanium (Ti). Coarse particles that were rich in chromium and tungsten (Figure 30 (a)) also were noted. The W-rich particles have been due to tool wear. W-Re-HfC instead of W-La₂O₃ will alleviate it in future processing.

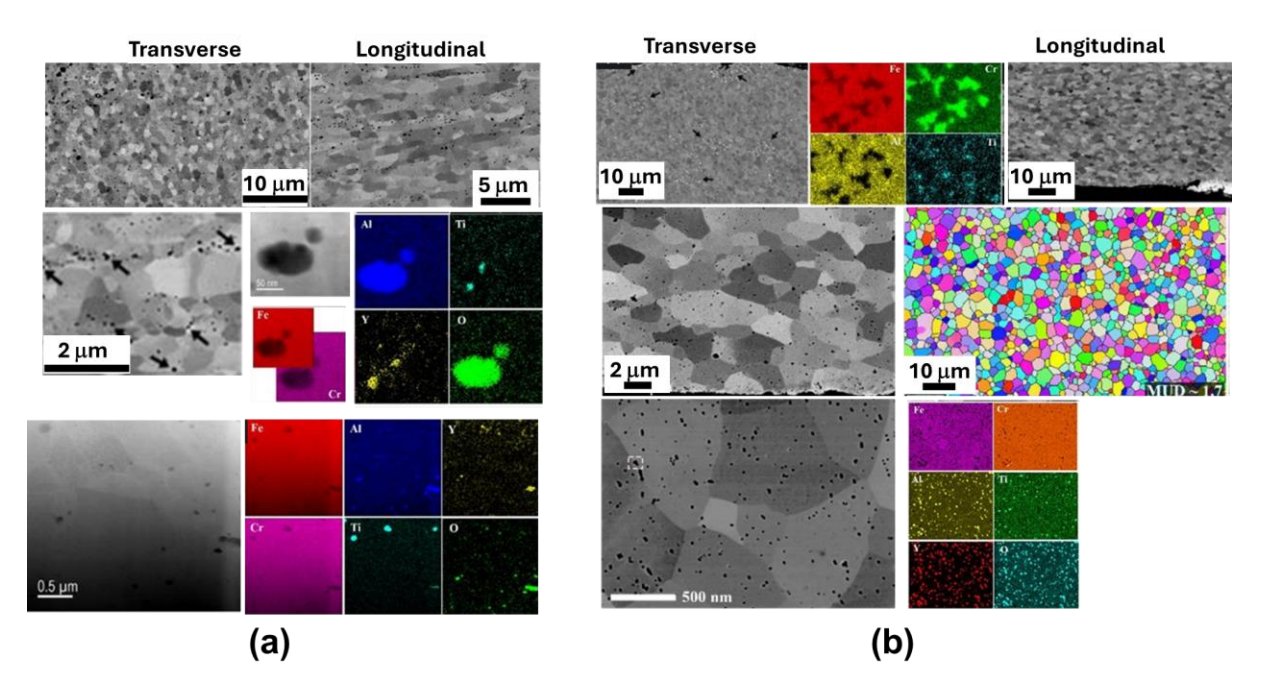


Figure 30. SEM micrographs comparing PM2000 steel microstructure in (a) as-received condition and (b) following ShAPE tube processing, demonstrating the evolution of grain structure and oxide particle distribution during thermomechanical processing.

In both the PM2000 base metal rod and ShAPETM samples, Al- and Y-rich secondary precipitates, Al_2O_3 and/or $(Al, Y)_2O_3$ type oxides, and elemental Ti-rich particles could be identified from electron microscopy analysis. This data also are consistent with reported data on the Al- and Y-rich oxide precipitate composition of YAlO $_3$ in PM2000 alloy (Jung et al. 2017). As shown by the precipitate size distribution (Figure 31a) and precipitates average sizes (Figure 31b), the precipitate size increases in the order of base metal to start to the middle of the ShAPE sample, while the end section of the ShAPE sample has smaller precipitate sizes than that of the middle section. The precipitate size in the middle and end sections of the ShAPE tube samples are twice the size of the base metal sample. The number density of precipitates is inversely proportional to the change of their size, The increase in the size of precipitates and decrease in their densities suggest ShAPE-induced growth of the secondary oxide particles without significantly affecting the overall level of oxidation. This suggests that ShAPE might be used to refine ODS particles, but further experimentation is required to verify this observation.

The average Vickers microhardness value for PM2000 base metal rod (longitudinal) sample was 321 HV. The maximum, minimum and standard deviation values were 329, 311, and 4 HV, respectively. These results showed that the hardness was quite uniform (i.e., standard deviation <4) across the sample (see Figure 32a). The average Vickers microhardness value for PM2000 base metal rod (transverse) sample was 329 HV and it is (Figure 32b) fairly similar to the longitudinal sample. The maximum, minimum and standard deviation values in the transverse sample were 361, 313, and 11 HV, respectively, with a greater higher end value.

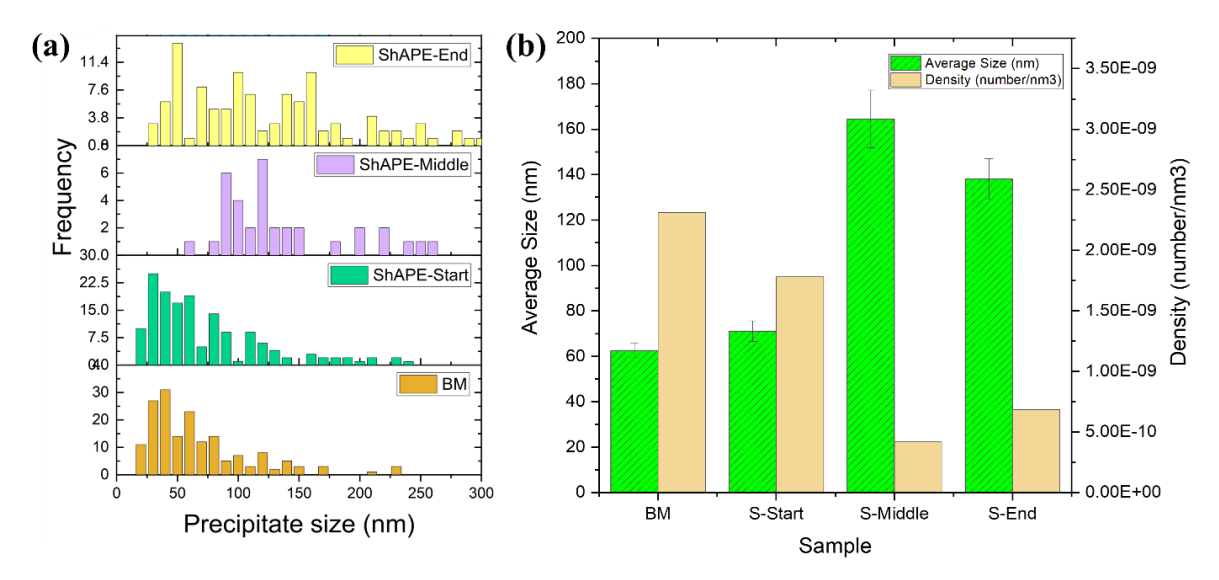


Figure 31. PM2000 base metal (rod) and ShAPE tube samples. (a) Precipitate size distribution and (b) average precipitate size and density distributions. BM, S-Start, S-Middle, and S-End denote base metal, start, middle, and end sections of the ShAPE tube.

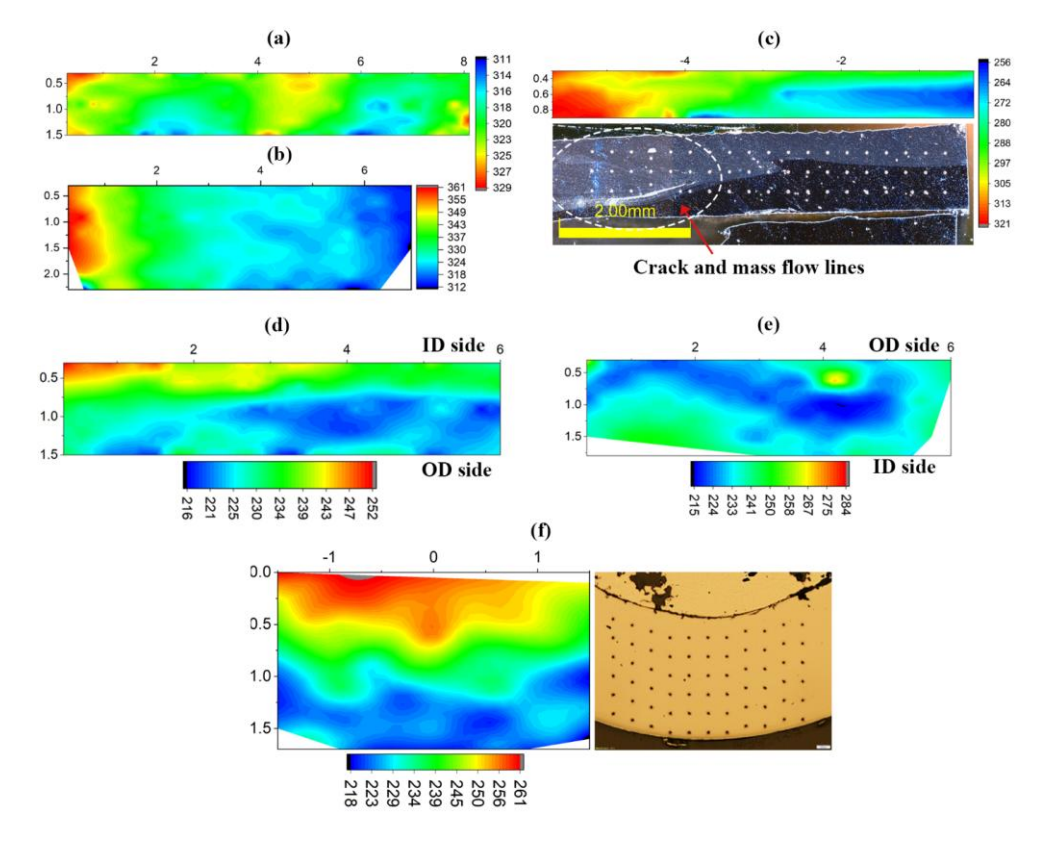


Figure 32. Vickers microhardness profile of PM2000 base metal rod. (a) Longitudinal sample; (b) transverse sample and ShAPE extruded samples in longitudinal direction: (c) start, (d) middle, (e) end, and (f) ShAPE extruded middle sample in transverse direction. Note that the color map shows the hardness in HV, while X and Y axes denote distance in millimeters.

4.4 ShAPE Manufactured 14YWT ODS Steel

As the 14YWT powder was mechanically alloyed and flakey and initial challenges were experienced for the sintering process as part of the earlier FFF work, we decided to use a densification process to produce the input billets (i.e., the feedstock) for the ShAPE equipment, and SPS was chosen for our first ODS SHAPE experimentation. Although ShAPE bar manufacturing from gas atomization reaction synthesized powder occurred, this will be the first direct manufacturing of tubing using 14YWT ODS steel powder.

The SPS sinter temperatures were kept lower than normal for full densification as to keep temperatures as low as possible for potential grain growth during densification as the full powder size-microstructure-manufacture-property relationships were not established at time of experimentation for these materials. Compared to the wrought PM2000, all the experiments with SPS billets as feedstock resulted in fractured tubes. This could be due to the porosity in the SPS consolidated feedstocks. An early conclusion is therefore that the stock material for the current feasibility shows that less than 97% dense feedstock is not sufficient for ODS materials for direct formation of tubes. However, another not previously established aspect that needs to be considered is how the bimodal grain sizes influence the consistency and flow during the extrusion process. Characterization of these extrudates could not yet be performed to determine if there are any differences in the ODS particle size or distributions after being exposed to the combined effect of SPS and ShAPE extrusion. Specifically, the third experiment using SPS billet 4 did not reach steady state; therefore, the microstructure resulting would not provide conclusive evidence yet.

Shape experimentation was performed with SPS billets 2, 4, and 3. The Shape processing characteristics of 14YWT SPS billets were significantly different from wrought PM2000 as shown in Figure 33, mainly due to the porosity and microcracks present in the SPS billets prior to extrusion. The results of the ShAPE experiments are shown in Figure 34. Comparing the second and third ShAPE experiments, ram velocity was increased by approximately five times during the third experiment as compared to the second experiment. The main reason for that change was to process at increased force to potentially increase consolidation. Both force and torque were higher during the third experiment as compared with the second run. Furthermore, oscillations in force and torque were noted, like the second run. Die temperature increased throughout the third run signifying that steady state was not reached; hence, further refinement in processing conditions to obtain a tube from SPS billets is needed. The die temperature near the start and end of 25 mm/min ram velocity was about 517°C and 1,176°C, respectively. For the fourth experiment, only ram velocity was changed to 15 mm/min. A maximum die temperature of 1,270°C was noted, and because of flash generation, the thermocouple was damaged around 5.5 mm plunge depth. Microstructural examinations of the SPS extruded experiments were not further detailed, as further optimization should be performed first.

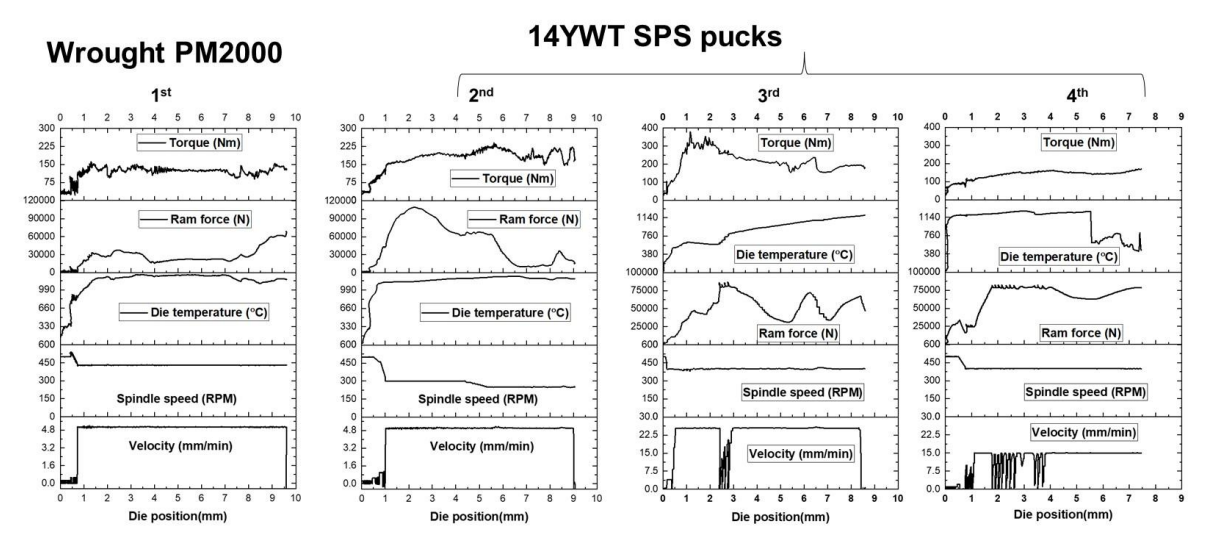


Figure 33. Summary of ShAPE process input and output for the four experiments completed for ODS steels



Figure 34. Comparative extruded images of the PM2000 and 14YWT SPS starting material

4.5 Conclusions and Recommendations on Feasibility Study on ShAPE Tube Forming of ODS Steel

This study provides first-of-a-kind results of direct tube formation using the ShAPE process for ODS steel material; previously only the bar form was successfully produced.

This study provides preliminary information on development of ShAPE tube forming of ODS directly from stock material, and not via an interim step of bar and pilgering as one of the current manufacturing methodologies. These experiments focused on determining sensitivity toward mechanically alloyed ODS powder, as previously, successful bar feedstock manufacturing was performed with highly specialized spherodized powder. The study investigation used two types of ODS steel feedstock billets: 1) uncrystallized ODS PM2000 alloy (Fe20Cr5Al) and 2) SPS billets fabricated for the AMMT program. The benefit of using this powder is that the result of the properties obtained from the AM techniques used in this study can be benchmarked. Because of the incomplete tube formation using the 14YWT SPS samples, no direct benchmarking could have been done as well as predicting the irradiation behavior.

The first ShAPE experiment completed on the PM2000 billet yielded an approximately 4-inch length of tube and shows in principle the feasibility of the direct tube fabrication in a single step while recognized that full steady-state conditions were not reached during the first experiment and that process optimization should still be performed on this specific material conditions. A detailed microstructural analysis—although showing variations between the start, middle, and end sections—shows that conditions towards the end were more consistent and can be built upon during next studies. However, the results—both in understanding the process parameters and behavior in relationship with the microstructural variations—can provide valid input to the modeling efforts, although not funded under the AMMT program, can minimize future experiments. Specific observations from the PM2000 extrudate tube are described below:

- Al- and Y-rich secondary precipitates, Al₂O₃ and/or (Al, Y)₂O₃ type oxides, and elemental Ti-rich particles could be identified from electron microscopy analysis.
- The presence of dispersoids with varying size were noted. The precipitate size increases during SHAPE processing to approximately double the base material size, although the precipitate sizes of the end section are smaller than the mid-section. The ShAPE tube exhibited equi-axed, recrystallized fine grain structure.
- The number density of precipitates shows an inverse proportionality to the change of their size, except for the bulky square-type Al-rich precipitates mostly identified at the end section of the ShAPE sample. The increase in the precipitate size and decrease in density suggest ShAPE-induced growth of the secondary oxide particles without significantly affecting the overall level of oxidation. This suggests that ShAPE might be used to refine ODS particles, but further experimentation is required to verify this observation. However, the moderate size and the highest density of bulky square-type precipitates observed at the end section of the extruded sample also suggest ShAPE-induced increase in the second phase precipitation. Therefore, decrease of temperature during the optimization of the process parameters needs to be prioritized.
- A slight reduction in hardness was noted due to complete recrystallization above 1,250°C processing temperature as compared to base metal, which was in a worked state.

Finally, the four ShAPE experiments conducted demonstrate feasibility regarding fabricability for ODS tube forming, although optimization for microstructure repeatability would need to receive attention with follow-up work. Therefore, the combination of results reported here—together with results from other studies by PNNL researchers on bar fabrication of ODS—provide the justification for early Technical Readiness Level feasibility.

From this work, we conclude that ShAPE processing of high-temperature materials is possible, and with different sets of tooling materials improved quality tubes can be obtained. Additionally based on the forces and torque used, the processing temperature can be decreased to maintain the size of dispersoids similar to low-temperature processing.

5.0 Feasibility Study Conclusions and Recommendations

This study described the feasibility of solid-state manufacturing methods for applications within the nuclear industry. Overall, three product forms were investigated, namely a honeycomb structure, flat and tubular samples, were manufactured to demonstrate the flexibility of product form. The study included investigation of two 14YWT ODS powder batches that provided information on the effect of different powder morphologies on manufacturability and two 316SS powders demonstrated the effect of powder size on manufacturability. One wrought bar stock of PM2000, a commercial ODS alloy, was also used to further showcase the flexibility in raw material (input product) form during the application of solid-state manufacturing methods. The main conclusions of each feasibility study are described below.

5.1 Conclusions and Recommendations on Cold Spray and Additive Friction Surfacing

The initial CS experiments using 316H SS powder size (such as laser powder directed energy deposition powder) were not sufficient to provide a full bonded structure. However, alternating CS with FSP resulted in an inherent bonded and dense structure. The application of AFS was demonstrated and shows promise for future near net shape manufacturing and bulk manufacturing of high strength and high temperature materials. Specific conclusions are listed below:

- Equiaxed ultrafine grain structure produces improved properties and corrosion resistance
- Potential economic cost cladding or local AM
- Amenable to solid phase alloying and functionally gradient chemistries/microstructures
- First attempt reduced grain size from ~27 to ~2 4 μ m. We anticipate ~1 to 1.5 μ m is achievable with process optimization.
- Boron-nitride particles from the PCBN FSP tool were unexpected and may indicate the tool is faulty and are not expected in future runs.
- Significant technology developed is required to prepare AFS for commercialization; however, this work has demonstrated the following:
 - AFS can create ultrafine grained builds of SS-316H using low-cost rod stock.
 - Conditions exist where interlayer boundaries are not readily visible, and grain structure is homogenous.
 - Results show that AFS is a feasible method for NNS LSAM of nuclear components with improved properties and cost compared to competing techniques.

5.2 Conclusion and Recommendations on FFF Evaluation

In this work, we demonstrated the feasibility of using FFF for fabricating parts from 316H SS and ODS steels. Both ODS steel and 316H custom filaments were fabricated with a powder loading of 65% and 62% respectively. Specific filament fabrication and printing parameters for each material type and powder were determined to achieve the successful printing and therefore show feasibility to use FFF for component manufacturing. However, process optimization for more dense parts is necessary and scalability needs further work.

The research results provided in this report provide evidence that it is feasible to print ODS steel as well as 316H SS using the FFF solid-state fabrication process with the following conclusions:

- The filament fabrication process and printing are sensitive for powder morphology, size, and size distribution mainly due to the flowability of the filament extrusion and the sinter effectiveness.
- Custom powder can be used for FFF; therefore, an in-house PNNL capability was developed enabling ODS and 316H SS powder loading techniques.
- Although effective printing and subsequent sintering did occur, further optimization is needed to fully fabricate structural sound components.

Successful printing and sintering were achieved, with the following key takeaways:

- FFF provides superior control over microstructural features such as equiaxed grain size and oxide particle distribution compared to laser-based AM methods.
- Powder characterization plays an essential role in achieving manufacturable filaments and structurally sound components.
- While promising, optimization of sintering processes and scalability is required for full adoption in nuclear-grade applications.

It is recommended that the next phase of development include the following:

- Process improvements for achieving denser and larger components through the detailing on the particle size distribution window, as well as impurity levels to ensure structural integrity
- Customization of the polymer composition to increase the powder loading of the filament, and potentially the modeling of the process to accelerate the particle loading optimization
- Expanded applications of FFF techniques for complex geometries and critical reactor components
- Comparative studies across other solid-state techniques (e.g., CS, shear-assisted processing) to determine optimal manufacturing methods for various materials.

5.3 Conclusions and Recommendations on ShAPE Evaluation

This study provides the first-of-a-kind results of direct tube formation though ShAPE for ODS steel material. Previously, only bar shapes have been successfully made. This study provides preliminary information on development of ShAPE tube forming of ODS directly from stock material, and not via an interim step of bar and pilgering as one of the current manufacturing methodologies. Main conclusions described below on the two input material sets:

- The first ShAPE experiment completed on the PM2000 billet yielded an approximately
 4-inch length of tube and shows in principle the feasibility of the direct tube fabrication in
 a single step while recognized that full steady-state conditions were not reached during
 the first experiment, and that process optimization should still be performed on this specific
 material conditions.
 - A detailed microstructural analysis, although showing variations between the start, middle and end sections, shows that conditions towards the end were more consistent and can be built upon during next studies. However, the results, both in understanding the process parameters and behavior in relationship with the microstructural variations,

- can provide valid input to the modeling efforts, although not funded under the AMMT program, can minimize future experiments. Specific observations from the PM2000 extrudate tube are described below:
- Al- and Y-rich secondary precipitates, Al₂O₃ and/or (Al, Y)₂O₃ type oxides, and elemental Ti-rich particles could be identified from electron microscopy analysis.
- The precipitate size increases during SHAPE processing to approximately double the base material size, although the precipitate sizes of the end section are smaller than the mid-section.
- The number density of precipitates shows an inverse proportionality to the change of their size, except for the bulky square-type Al-rich precipitates mostly identified at the end section of the ShAPE sample. The increase in the precipitate size and decrease in density suggest ShAPE-induced growth of the secondary oxide particles without significantly affecting the overall level of oxidation. This suggests that ShAPE might be used to refine ODS particles, but further experimentation is required to verify this observation. However, the moderate size and the highest density of bulky square-type precipitates observed at the end section of the extruded sample also suggest ShAPE-induced increase in the second phase precipitation.
- Compared to the wrought PM2000, all the experiments with SPS Billets as feedstock resulted in fractured tubes. This could be due to the porosity in the SPS consolidated feedstocks. An early conclusion is therefore that the stock material for the current feasibility shows that less than 97% dense feedstock is not sufficient for ODS materials for direct tube forming. However, another aspect that needs to be considered that has not been established, is how the bimodal grain sizes influence the consistency and flow during the extrusion process. Characterization of these extrudates could not be performed yet to determine if there are any differences in the ODS particle size or distributions after being exposed to the combined effect of SPS and ShAPE extrusion. Specifically, the third experiment using SPS billet 4 did not reach steady state; therefore, the microstructure resulting would not provide conclusive evidence yet.

Finally, the four ShAPE experiments conducted show feasibility regarding fabricability for ODS tube forming was shown, although optimization for microstructure repeatability would need to receive attention with follow-up work; therefore, the combination of results reported here, together with the separate studies by other PNNL researchers on bar fabrication of ODS, provide the justification for level 3-4 Technical Readiness Level feasibility.

6.0 Application Space for Solid-State Processing in the Nuclear Industry

Solid-state and specifically solid-phase processing enables process intensification, allowing for new phase forming and microstructural refinement/homogenization which can result in superior properties and reduced cost. ODS materials are good candidates to demonstrate these advantages.

Solid-phase processing techniques have furthermore the potential to decrease the dependency on highly specializing powder fabrication with dispersoid materials, as direct manufacturing may be possible due to the intensification of the processes. Among other benefits, upscaling and larger NNS products are possible and typical applications. As the domain space is more frequently exposed to high-strength materials, the Technical Readiness Level levels will increase, and therefore, applications will become more attractive for industry players. The benefits and application domains for various solid state manufacturing processes are shown in Table 4.

The advancements described in the report hold significant promise for both nuclear energy systems and broader manufacturing applications under the broad categories of:

- Safety Improvements: Enhanced microstructural control leads to higher mechanical strength and irradiation resistance, which is critical for reliable nuclear materials.
- *Economic Benefits:* Reduction in waste and optimization of manufacturing processes result in lower production costs.
- Sustainability: Solid-state AM methods minimize material waste by enabling near-net shapes directly from powder feedstock; operational efficiency also is enhanced.
- Enhancement of properties: Developing advanced AM techniques could lead to improvements in microstructural control, grain shape, and oxide particle optimization.
- Manufacturing route for high melting point materials and provide enhancement of properties compared to melt processes:
 - Fabrication of nuclear grade components such as fuel cladding and structural elements for high-temperature reactors.
 - Fabrication for high-strength dispersoid materials and bulk manufacturing for high entropy materials
 - Micro-reactors and outer space reactor applications (i.e., development of ODS steels with enhanced strength-to-weight ratios for space exploration)
 - Wider manufacturing deployment in industries requiring precision-engineered parts, such as energy generation and automotive manufacturing.

Table 4. Applications space and benefits for solid-state manufacturing processes

	Process Intensification	Enable Superior Properties
ShAPE	 Tubing and pipe material Cladded tube or pipe material Functionally graded material and/or multi material Single step process from low-cost billet or powder Includes cladding and functionally graded CNC controlled, fully automated Cost competitive 	 Microstructural control Solid phase alloying enables Refine and homogenize distribution of strengthening particles Improved corrosion and mechanical and creep performance anticipated for high temperature materials for interest Improved irradiation resistance
FFF	 Small component with fine tolerances Functionally graded material and/or multi material Can perform lattice structures, but low Technical Readiness Level for high-strength and high-melting-point materials Scaling up for production rate is possible, nozzle technologies need further development Internal cavities, design flexibility 	 High melting point material sintering after forming enables difficult to form small features Magnetic materials, as well as dissimilar material bonding or possible to manufacture without interaction, lead to unique conductivity designs Improved irradiation resistance
AFS	 Accelerate materials R&D Rapid fabrication of novel chemistries (ODS, refractory) Functionally graded chemistry and microstructures Enable superior design NNS LSAM or cladding Cost competitiveness: Improved economics Feedstock is 3-10x less expensive than powder or weld wire With process development anticipate feed rates greater than 3x the nearest competitor for NNS AM of steels 	 Equiaxed ultrafine grain structure Wear resistance Corrosion resistance for MSR or other applications Alloying elements mixed and refined in microstructure Improved irradiation resistance
HPCS	 Accelerate materials R&D Rapid screening of new alloys Functionally graded materials 	 Enable superior design Induces compressive residual stress: fatigue performance Wear resistance Corrosion barrier for MSR Environmental barrier
FSW	 Cost competitiveness: Improved economics Coating, Cladding or NNS AM Magnetostrictive condition monitoring at high temperatures Waste canisters Life Extension for Next Gen and Existing fleet Improved performance and economics Life extension/Lifecycle In-situ repair 	 Local grain refinement and homogenization Fully automated, single pass welds with no detrimental HAZ Dissimilar material joining Improved irradiation resistance

7.0 References

ASTM. 2020. "Standard Test Method for Particle Size Distribution of Metal Powders and Related Compounds by Light Scattering." https://www.astm.org/b0822-20.html.

ASTM. 2022. "Standard Test Method for Microindentation Hardness of Materials." https://www.astm.org/e0384-22.html.

Azushima, A., Kopp, R., Korhonen, A., et al., 2008. "Severe plastic deformation (SPD) processes for metals." CIRP Annals 57(2) 716-735.

Bhattacharyya M, A Kundu, KS Raja, J Darsell, S Jana and I Charit. 2021. "Processing-microstructure-property correlations for temperature-controlled friction stir welding of 304L SS plates." *Materials Science and Engineering: A* 804:140635. DOI: https://doi.org/10.1016/j.msea.2020.140635.

Burns Carolyne A, Saumyadeep Jana, Amrita Lall, Zachary C Kennedy, Michelle D Fenn, Joshua A Silverstein, Lorraine M Seymour, Isabella J van Rooyen; "Preliminary Characterization and evaluation on FFF Manufactured 316H and ODS Steels", PNNL-34985, September 2023, (Burns et al. 2023).

Garcia D, T Wang, JD Escobar, M Pole, X Ma and KA Ross. 2024. "In-situ measurement and control of the tool-workpiece interface temperature during friction stir processing of 304/304L stainless steel." *Materials Today Communications* 38:107672. DOI: https://doi.org/10.1016/j.mtcomm.2023.107672.

Gwalani B, M Song, J Silverstein, J Escobar, T Wang, M Pole, K Johnson, BK Jasthi, A Devaraj and K Ross. 2022. "Thermal stability and mechanical properties of cold-sprayed Nickel-Yttria coating." *Scripta Materialia* 207:114281. DOI: https://doi.org/10.1016/j.scriptamat.2021.114281.

Jiang X, N Overman, N Canfield and K Ross. 2019. "Friction stir processing of dual certified 304/304L austenitic stainless steel for improved cavitation erosion resistance." *Applied Surface Science* 471:387-393.

Jung, H. J.; Edwards, D. J.; Kurtz, R. J.; Yamamoto, T.; Wu, Y.; Odette, G. R. Structural and chemical evolution in neutron irradiated and helium-injected ferritic ODS PM2000 alloy. Journal of Nuclear Materials 2017, 484, 68-80.

Komarasamy M., Lei Li, B. Taysom, B. Taysom, A. Soulami, G. Grant, D.Herling and S. Whalen. 2022. "Co-Extrusion of Dissimilar Aluminum Alloys via Shear-Assisted Processing and Extrusion." Light Metals 2022, 308-313

Li, M., D. Andersson, R. Dehoff, A. Jokisaari, I. van Rooyen, D. Cairns-Gallimore,2022a. "Advanced Materials and Manufacturing Technologies (AMMT) 2022 Roadmap." ANL-23-12, September 2022.

Moridi A, SM Hassani-Gangaraj, M Guagliano and M Dao. 2014. "Cold spray coating: review of material systems and future perspectives." *Surface Engineering* 30(6):369-395. DOI: 10.1179/1743294414Y.0000000270.

References 49

Ross KA and M Alabi. 2019. *Update on Investigations of Viability of Cold Spray and FSW as a Spent Nuclear Fuel Dry Storage Canister Mitigation Tool*. Pacific Northwest National Lab.(PNNL), Richland, WA (United States). DOI: 10.2172/1580110. Available at https://www.osti.gov/servlets/purl/1580110.

Ross KA, JP Lareau, SW Glass and RM Meyer. 2021. *Assessment of Cold Spray Technology for Nuclear Power Applications*. Washington, D.C.: U.S. Nuclear Regulatory Commission. Available at

https://adamswebsearch2.nrc.gov/webSearch2/main.jsp?AccessionNumber=ML21263A107. ADAMS Accession No. Adams Accession No. ML21263A107.

Silva, C.M., M. Komarasamy, J. D. Escobar, S. Tripathi, R. Prabhakaran, Q. R. S. Miller, T. A. Ajantiwalay, M. J. Olszta, I. J. van Rooyen. 2024a, A discussion on microstructural and mechanical characteristics of ShAPE extruded PM2000 FeCrAl tubes, TMS2024, March 3–7, 2024, Hyatt Regency Orlando, Orlando, Florida, USA (Silva et.al. 2024a)

Silva et.al. 2024b, Journal Publication: Chinthaka M Silva, Mageshwari Komarasamy, Julian D Escobar, Shalini Tripathi*, Ramprashad Prabhakaran, Quin R S Miller, Tanvi A Ajantiwalay, Matthew J Olszta, Isabella J Van Rooyen, "Manufacturing of oxide dispersion strengthened Fe-Cr-Al alloy using a nonconventional extrusion process", Accepted in JMEP, September 2025

Tuncer, N. and A. Bose. "Solid State Manufacturing: A Review." 2020. JOM, Vol. 72, No. 9, 2020.

van Rooyen Isabella, Mageshwari Komarasamy, Chinthaka Silva, Shalini Tripathi, Julian Atehortua, Mayor Pole, Tanvi Ajantiwalay, David Garcia, Quin R S Miller, Matthew Olszta, Ramprashad Prabhakaran, Tianhao Wang; "Preliminary Characterization and Evaluation on ShAPE Manufactured 316H and ODS Steels", M3CR-22PN0402023, PNNL-36737, September 2024, (Van Rooyen et al. 2024)

Whalen, S., N. Overman, V. Joshi, T. Varga, D. Graff, and C. Lavender. 2019. "Magnesium alloy ZK60 tubing made by Shear Assisted Processing and Extrusion (ShAPE)." Mater. Sci. Eng. A. 755: 278–288.

Zhang, D., J.T. Darsell, J. Wang, X. Ma, G.J. Grant, I.E. Anderson, J.R. Rieken, D.J. Edwards, W. Setyawan, T.J. Horn, G.R. Odette. 2022. "No ball milling needed: Alternative ODS steel manufacturing with gas atomization reaction synthesis (GARS) and friction-based processing." Journal of Nuclear Materials, Volume 566, 1 August 2022, 153768 https://www.sciencedirect.com/science/article/pii/S0022311522002550?via%3Dihub

VRC Metal Systems. 2020. "COLD SPRAY VS THERMAL SPRAY – AN OVERVIEW." Accessed July 13,2020. Available at https://www.vrcmetalsystems.com/blog-post/cold-spray-vs-thermal-spray/.

References 50

Pacific Northwest National Laboratory

902 Battelle Boulevard P.O. Box 999 Richland, WA 99354

1-888-375-PNNL (7665)

www.pnnl.gov